

# Energy Technology

Generation, Conversion, Storage, Distribution

## Accepted Article

**Title:** Recent Advancement in Metal Halide Based Perovskite Light Emitting Diodes

**Authors:** DINESH KABRA, Naresh Kumar Kumawat, and Dhritiman Gupta

This manuscript has been accepted after peer review and appears as an Accepted Article online prior to editing, proofing, and formal publication of the final Version of Record (VoR). This work is currently citable by using the Digital Object Identifier (DOI) given below. The VoR will be published online in Early View as soon as possible and may be different to this Accepted Article as a result of editing. Readers should obtain the VoR from the journal website shown below when it is published to ensure accuracy of information. The authors are responsible for the content of this Accepted Article.

**To be cited as:** *Energy Technol.* 10.1002/ente.201700356

**Link to VoR:** <http://dx.doi.org/10.1002/ente.201700356>

# Recent Advancement in Metal Halide Based Perovskite Light Emitting Diodes

Naresh K. Kumawat,<sup>1</sup> Dhritiman Gupta,<sup>\*2</sup> Dinesh Kabra<sup>\*1</sup>

<sup>1</sup>Department of Physics, Indian Institute of Technology Bombay Powai, Mumbai-400076  
(India)

E-mail: [dkabra@iitb.ac.in](mailto:dkabra@iitb.ac.in)

<sup>2</sup>School of Advanced Sciences, Department of Physics, Vellore Institute of Technology,  
Vellore-632014, Tamil Nadu, India

E-Mail: [dhritiman.gupta@vit.ac.in](mailto:dhritiman.gupta@vit.ac.in)

Accepted Manuscript

**Naresh Kumar Kumawat** is a Ph.D. student at the laboratory of Hybrid Optoelectronic Devices at Department of Physics, Indian Institute of Technology Bombay (IITB) India, under the supervision of Prof. Dinesh Kabra. He received his M.Tech. Degree in Solid State Materials from Department of Physics, Indian Institute of Technology Delhi (India) in 2013. His current work is on metal halide perovskite semiconductors for optoelectronic device application e.g. perovskite light emitting diodes (PeLEDs), solar cell (SC).



**Prof. Dhritiman Gupta** received M.Sc degree in Physics from University of Calcutta, Kolkata, India in 2002 and Ph.D from Jawaharlal Nehru Centre for Advanced Scientific Research (JNCASR), Bangalore in polymer based optoelectronics in the year 2009. Prior to joining as Assistant Professor in Vellore Institute of Technology, Vellore, Tamil Nadu (India) he was a postdoctoral fellow in University of Cambridge and Eindhoven University of Technology (TU/e). His research interest is organic polymer, metal oxides and Si based hybrid photovoltaics with focus on air-stability and large-area application. He is also involved in modelling single-junction and multi-junction solar cells.



**Prof. Dinesh Kabra** is at present Associate Professor in the Department of Physics at IITB, Mumbai (India). Before joining IITB in 2012, he was a Herchel Smith Research Fellow in Cavendish Laboratory, University of Cambridge, UK. He is also an honorary postdoctoral fellow of Trinity Hall College, University of Cambridge. He did his PhD in 2007 from JNCASR, Bangalore (India) to understand photo-induced charge carrier transport length scales in model conjugated polymer systems. His current research interest involves solution processable inorganic & organic molecular/ metal halide based perovskite semiconductors to understand their charge transport & photo-physics and transfer that knowledge to design high performance optoelectronic devices.



## Abstract

Metal halide perovskite materials are crystalline semiconductors which can be processed at room temperature via solution processable deposition techniques. In few years, perovskite based solar cell efficiency has seen a huge boost from 3% to 22.1%. These are direct band gap materials which makes them potential candidate for other optoelectronic device applications such as photo detector, light emitting transistor and light emitting diode. In this review, we discuss the present scenario in the research and development of perovskite light emitting diodes (PeLEDs) based on metal halide perovskite semiconductors with an emphasis on size of the crystallites and its consequence on optical properties, device architectures and corresponding PeLED performance parameters. A uniform pin-hole free morphology with small grain size is essential for high performance PeLED. For this purpose, a *p-i-n* type device architecture with PEDOT:PSS *p*-type layer has been found more suitable over the *n-i-p* type. In PeLEDs based on the bulk phase of the perovskites, the average size of the crystallites is in the range ~ 100 - 500 nm. The efficiency can be improved further by using perovskite nanoparticles with size < 100 nm. Color of the emitted light from these materials is tuned over a wide range, NIR (775 nm) to near-UV (410 nm), simply by changing the halide ion and the stoichiometric ratio between halide ions in mixed halide type perovskites. Change of stoichiometry also affects the structural properties and the final film morphology which in turn influences the radiative and non-radiative recombination rates of the charge carriers and hence the device performance. Furthermore, we also provide recent parallel developments in inorganic perovskite nano-crystals based PeLEDs, which is complimenting the efforts being made in hybrid PeLEDs.

**Keywords:** Metal halide perovskites, Structural properties, Photoluminescence, Perovskite light emitting diodes.

## 1. Introduction

Light emitting diodes (LEDs) are basic optoelectronics device which are regularly being used in display technology, medical science and optical communication. LED based lighting technology is economically more attractive due to its high intensity light output at low operating voltage coupled with low heating losses and long lifetime.<sup>[1]</sup> Electroluminescence (EL) was first observed in silicon carbide (SiC) by Henry Round in 1907, who reported yellow colored EL at high voltage levels.<sup>[2,3]</sup> A follow up of this work was reported by Oleg Lossev *et. al.* in 1927.<sup>[4]</sup> However, more practical cases of LEDs were reported only in 1955 when Braunstein *et. al.* reported infrared LED, operating at room temperature and at 77K, using simple diode structure of GaAs, InP, GaSb and SiGe.<sup>[5]</sup> Soon after this discovery, in 1961 Biard *et. al.* reported the LED device using GaAs with diffused Zn p-n junction. This GaAs LED had efficient emission in infrared region (900 nm) <sup>[6]</sup> and it was the first commercialized LED. Subsequently, in 1972 Holonyak *et. al.* reported visible red LED using Ga(As<sub>1-x</sub>P<sub>x</sub>).<sup>[7]</sup> In addition to red and green, for production of white light, blue EL was required. In 1994 Shuji Nakamura and coworkers reported InGaN based bright blue LED and paved the way for white light generation. He was awarded Nobel Prize in the year 2014 for his discovery.<sup>[8]</sup>

Color of EL can be controlled by proper tuning of bandgap. In inorganic semiconductors, band gap can be tuned from UV-Vis to NIR and it is done by using alloy method, (see **Figure1**). Inorganic semiconductors have long life time and stability, but still, these are color impure (e.g. GaN and InGaN based LEDs have green emission band along with the characteristic blue emission) <sup>[9,10,11]</sup> and require expensive high temperature, high vacuum based processes for fabrication. Meanwhile researchers started working on low-cost solution processable organic semiconductors (polymers and small molecules) as emissive layer for LEDs (Organic LEDs or OLEDs). In 1950s EL was observed by Bernanose *et. al.* using Acridine orange (C<sub>17</sub>H<sub>19</sub>N<sub>3</sub>)

[12,13,14] although the reliability of the device was poor. In 1960 Kallmann *et. al.* reported EL from organic crystal, anthracene, at very high AC voltage (500-1500V).<sup>[15]</sup> First report of EL in organic polymer, Poly N-Vinylcarbazole (PVK) was in 1985 from Roger Partridge of National Physical Laboratory. This device did not attract great attention due to poor performance. But soon afterwards, two milestone discoveries in the field of organic LEDs were reported. First one by Tang *et. al.* in 1987, where EL was observed in organic small molecules<sup>[16]</sup> and the second one by the group in Cavendish Laboratory led by Richard Friend in the year 1990, when Burroughes *et. al.* reported high efficiency green LED using PPV polymer.<sup>[17]</sup>

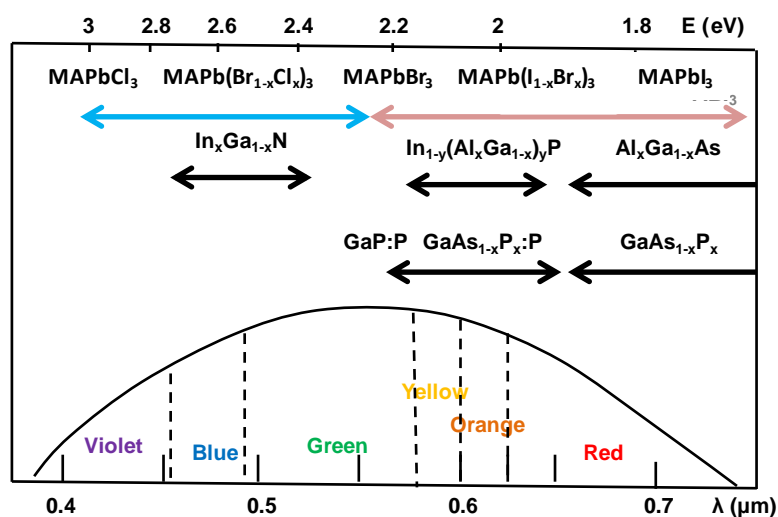


**Figure 1** Inorganic semiconductors and metal halide perovskite materials (with generic formula  $\text{MAPbX}_3$ , wherein MA = methylammonium ( $\text{CH}_3\text{NH}_3$ ); X = Cl, Br or I or mixed halide) and their corresponding light emission wavelength along with the eye response curve. Using metal halide perovskite materials, band gap can be tuned from NIR to UV-Vis and span the same colour window as spanned by inorganic ones.

Since then, enormous research has been done on OLEDs and at present OLEDs are commercialized in various display based industries. Despite its impressive success, OLED technology is still struggling to become competitive with inorganic LEDs. Short lifetime and low efficiency of blue OLEDs are the main hurdles to be overcome.<sup>[18]</sup>

Recently, metal halide based perovskite materials with generic formula  $\text{CH}_3\text{NH}_3\text{PbX}_3$  (wherein  $X = \text{Cl}, \text{Br}, \text{I}$  or any mixed halide) has boosted photovoltaic energy conversion efficiency to a great extent. Within five years, power conversion efficiency (PCE) in perovskite solar cells has reached 22.1% from a very modest 3.4%.<sup>[19]</sup> Due to high absorption coefficient ( $\alpha \approx 10^5 \text{ cm}^{-1}$ ),<sup>[20]</sup> long charge carrier diffusion length ( $L_D > 1 \mu\text{m}$ ),<sup>[21]</sup> high mobility ( $\mu \sim 1\text{-}10 \text{ cm}^2/\text{V-s}$ )<sup>[22]</sup> and tunable optical bandgap (from UV-visible to NIR),<sup>[23]</sup> these class of materials are now extensively being investigated for their application in solar cell. According to principle of detail balance a good solar cell material can become a good LED material and vice versa when the light absorption and emission properties are compared. A good solar cell operating under open circuit condition should have only radiative recombination channels active and all the non-radiative channels suppressed. Perovskite materials manifest this reciprocity efficiently where both devices, solar cells and LEDs, benefit from the high photoluminescence quantum efficiency (PLQE), albeit under high excitation intensities.<sup>[24]</sup> Historically, 2D layered perovskites were investigated for LED application. However, EL was observed only at low temperatures ( $\sim 77\text{K}$ ), restricting its application in real life.<sup>[25,26,27]</sup> Using 3D perovskites, Schmidt *et al.* reported for the first time the EL observed at room-temperature. It remained unnoticed until the next report in 2014 on room-temperature operation of multi-color (NIR, red and green) metal halide perovskite-based LEDs by Tan *et al.*<sup>[28,29]</sup> The green LED of Tan *et al.* demonstrated external quantum efficiency (EQE) of 0.1%. Since this very recent discovery, a huge advancement has been made in the field of perovskite based LED over short span of time. So far, highest reported EQE for near-IR and green PeLEDs are 10.4% and 10.4% respectively.<sup>[30,31]</sup> Blue LEDs reported for the first time by our group<sup>[32]</sup> and also by Sadhalana *et al.*<sup>[33]</sup> and Li *et al.* (using inorganic nano-crystal approach) has lower EQE value of 0.004% at the initial stages.<sup>[34]</sup> Nevertheless, these discoveries set the foundation for white light generation using perovskite materials, a crucial requirement for display technology.<sup>[35]</sup> In this

review, we highlight recent progresses in metal halide based PeLEDs, mainly the perovskites with methyl ammonium ( $\text{MA} = \text{CH}_3\text{NH}_3^+$ ) and lead ( $\text{Pb}^{2+}$ ) metal cations, giving emphasis on the structural properties and consequent optical properties, different device architectures and the corresponding performance parameters.

## 2. Structural Properties

Metal halide perovskite materials are designated by generic formula  $\text{MAPbX}_3$  ( $\text{CH}_3\text{NH}_3\text{PbX}_3$ ) where the X anions are halides,  $\text{Cl}^-$ ,  $\text{Br}^-$  or  $\text{I}^-$  or mixed halides such as  $\text{IBr}$ ,  $\text{BrCl}$ ,  $\text{ICl}$  or  $\text{IBrCl}$ . In a crystal unit cell, MA cations are situated at the corner sites,  $\text{Pb}^{2+}$  cations are located at the body center and X anions are at the face-centers.  $\text{Pb}^{2+}$  cations are surrounded by 6 anions (X) and thus have coordination 6, while MA-cations have coordination 12 (see in **Figure 2a**).<sup>[36, 37, 38,39]</sup> Estimation of formability of stable crystal structure of perovskite is based on Goldschmidt tolerance factor.<sup>[40]</sup>

$$t = (R_{\text{MA}} + R_{\text{X}})/[\sqrt{2}(R_{\text{Pb}} + R_{\text{X}})]$$

Wherein  $R_{\text{MA}}$ ,  $R_{\text{Pb}}$ , and  $R_{\text{X}}$  are the effective ionic radii for the ions MA, Pb, and X respectively. For formation of ideal cubic structure this factor should be  $0.89 < t < 1$  for oxide perovskites<sup>[41]</sup> and should be  $0.85 < t < 1.11$  for halide perovskites.<sup>[42,43,44]</sup> Outside this tolerance range, for  $t < 1$ , octahedral tilting is expected. To further improve the predictability of formation of perovskite crystal structure, an additional parameter, called the octahedral factor ( $\mu$ ) was introduced by Li *et. al.*<sup>[42]</sup> Octahedral factor is given by the ratio of Pb cation to the X anion,  $\mu = R_{\text{Pb}}/R_{\text{X}}$ , and therefore it provides direct information of the  $[\text{PbX}_6]$  octahedron. Halide perovskite formation occurs for  $\mu > 0.442$ , whereas below this value  $[\text{PbX}_6]$  octahedron becomes unstable and a perovskite structure does not form. The  $t$  and  $\mu$  factors have been calculated for  $\text{MAPbCl}_3$ ,

MAPbBr<sub>3</sub> and MAPbI<sub>3</sub> (**Table-1**). As the ionic radii increases from Cl to I, the *t* factor decreases indicating increasing deviation from ideal cubic crystal structure. [45,46]

**Table1.** Estimation of *t*- $\mu$  factors for three different MAPbX<sub>3</sub> type perovskite materials.

$R_{Pb}$	$R_X$	$R_{MA}$	<i>t</i>	$\mu$
Pb <sup>2+</sup> (1.19 Å)	Cl <sup>-</sup> ( $R_{Cl}$ = 1.81 Å)	CH <sub>3</sub> NH <sub>3</sub> <sup>+</sup> ( $R_{MA}$ = 1.8 Å)	0.85	0.65
	Br <sup>-</sup> ( $R_{Br}$ = 1.96 Å)		0.84	0.61
	I <sup>-</sup> ( $R_I$ = 2.20 Å)		0.83	0.54

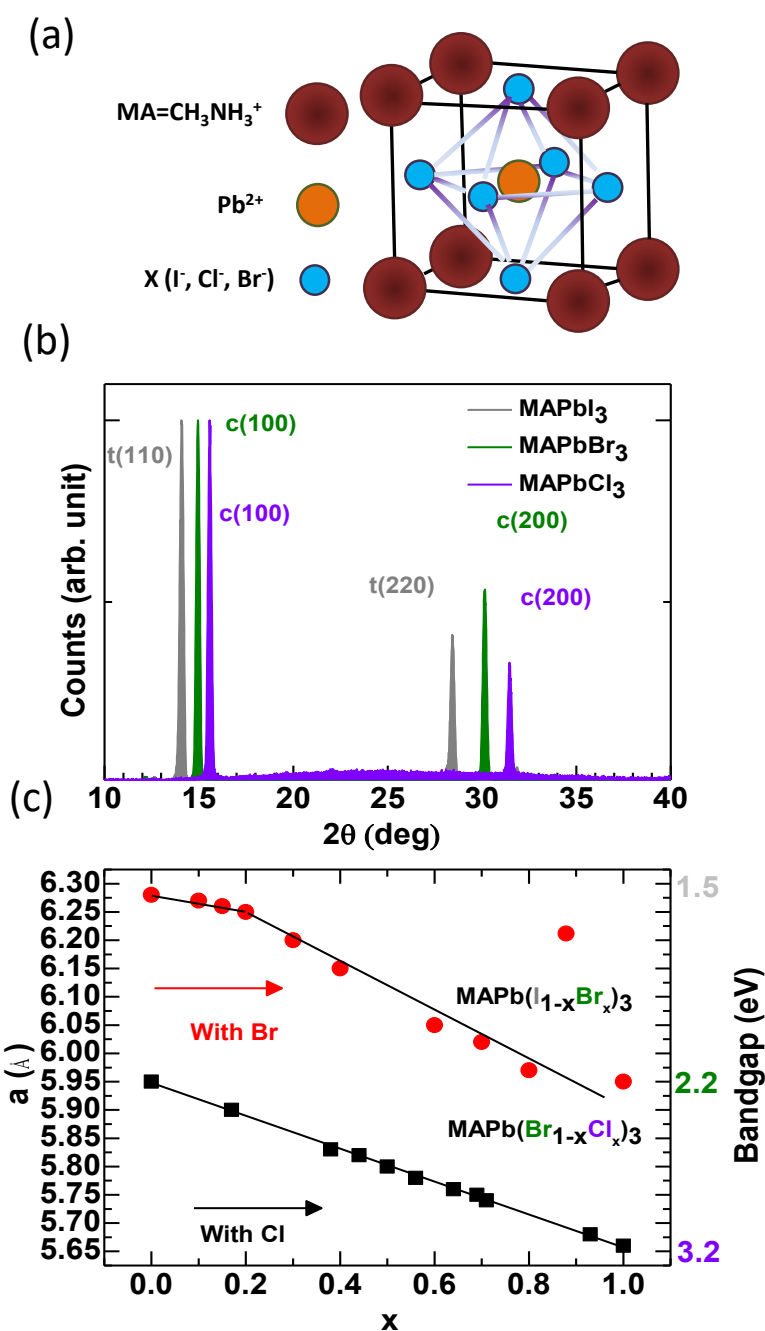


**Figure 2 (a)** Standard crystal structure of perovskite materials  $\text{MAPbX}_3$  where MA and X are  $\text{CH}_3\text{NH}_3^+$  or monovalent metal ( $\text{Cs}^+$ ) and halogen ( $\text{Cl}^-$ ,  $\text{Br}^-$  or  $\text{I}^-$ ) respectively. **(b)** Characteristic XRD peaks of  $\text{MAPbCl}_3$ ,  $\text{MAPbBr}_3$  and  $\text{MAPbI}_3$  **(c)** Lattice parameter and bandgap as a function of molar concentration of Cl and Br in mixed-halide type perovskites. [32, 38,47, 48]

At room temperature  $\text{MAPbCl}_3$  and  $\text{MAPbBr}_3$  both has cubic crystal structure whereas  $\text{MAPbI}_3$  has tetragonal crystal structure. [47,49] The corresponding x-ray diffraction (XRD) peaks are shown in **Figure 2b**. [50,51] XRD peaks are shifted towards low diffraction angle as deviation from cubic structure increases (from Cl to I). These materials have other phase also but those (tetragonal, orthorhombic) exist only at low temperature. [52] Well-defined and sharp XRD-peaks suggest that perovskites are crystalline in nature with long-range order. Upon changing the ratio of halide ion in mixed-halide type perovskites, such as,  $\text{MAPb}(\text{Br}_{1-x}\text{Cl}_x)_3$ ,  $\text{MAPb}(\text{I}_{1-x}\text{Br}_x)_3$ ,  $\text{CsPb}(\text{Br}_{1-x}\text{Cl}_x)_3$  and  $\text{CsPb}(\text{I}_{1-x}\text{Br}_x)_3$  lattice parameter and bandgap are modified without affecting the crystallinity. [32,39,48] **Figure 2c** shows change in lattice parameter and bandgap for  $\text{MAPb}(\text{Br}_{1-x}\text{Cl}_x)_3$  and  $\text{MAPb}(\text{I}_{1-x}\text{Br}_x)_3$  perovskite systems as a function of varying halide molar ratio. For  $\text{MAPb}(\text{Br}_{1-x}\text{Cl}_x)_3$  perovskite system, a linear variation of lattice parameter is obtained throughout the halide composition ( $x = 0$  to  $1$ ) mainly because, both  $\text{MAPbCl}_3$  and  $\text{MAPbBr}_3$  perovskites have cubic crystal structure at room temperature. [32] But  $\text{MAPb}(\text{I}_{1-x}\text{Br}_x)_3$  perovskite displays two slopes which is mainly attributed to the tetragonal crystal structure of  $\text{MAPbI}_3$ . Below  $x = 0.20$  crystal structure of  $\text{MAPb}(\text{I}_{1-x}\text{Br}_x)_3$  is tetragonal and above  $x = 0.20$  it becomes cubic. [48,53] In both systems lattice parameter decreases monotonically as chlorine and bromine concentration increases and thus affects the bandgap ( $E_g$ ) (since,  $E_g \sim 1/a$ , where, 'a' is lattice parameter). [54] Additionally, increasing the concentration of chlorine ions, not only affects the lattice constant, it also greatly enhances the grain size of the perovskite [32,49,55] and increases photoluminescence lifetime. [21,56] Hence the interplay between stoichiometry, optical bandgap and crystal grain size and their effect on electronic and optical property is rather

complex and is a subject of intense research. In the next section we discuss the optical properties of the perovskites which is relevant to the LED based research in the light of grain size effect and some of recent findings in this direction.

### 3. Optical Properties

#### 3.1 Tuning optical bandgap in mixed halide perovskite:

Perovskites materials are strong light absorbing semiconductors ideally suited for photovoltaic technology. Moreover, additional features are in absorption spectra of these materials such as sharp absorption edge indicates the presence of direct band gap with minimal disorder.

**Figure 3a** shows absorbance spectra of tri and mixed perovskite materials. Metal Halide perovskites, MAPbCl<sub>3</sub> or CsPbCl<sub>3</sub>, MAPbBr<sub>3</sub> or CsPbBr<sub>3</sub> and MAPbI<sub>3</sub> or CsPbI<sub>3</sub> have band gap of 3.1 eV, 2.3 eV and 1.6 eV or 1.8 eV, respectively.<sup>[32,39,48]</sup> These values come from the energy difference between (Pb)6s(X)np(VBM) and (Pb)6p(CBM) orbitals; wherein X = Cl, Br or I.<sup>[57, 58]</sup>

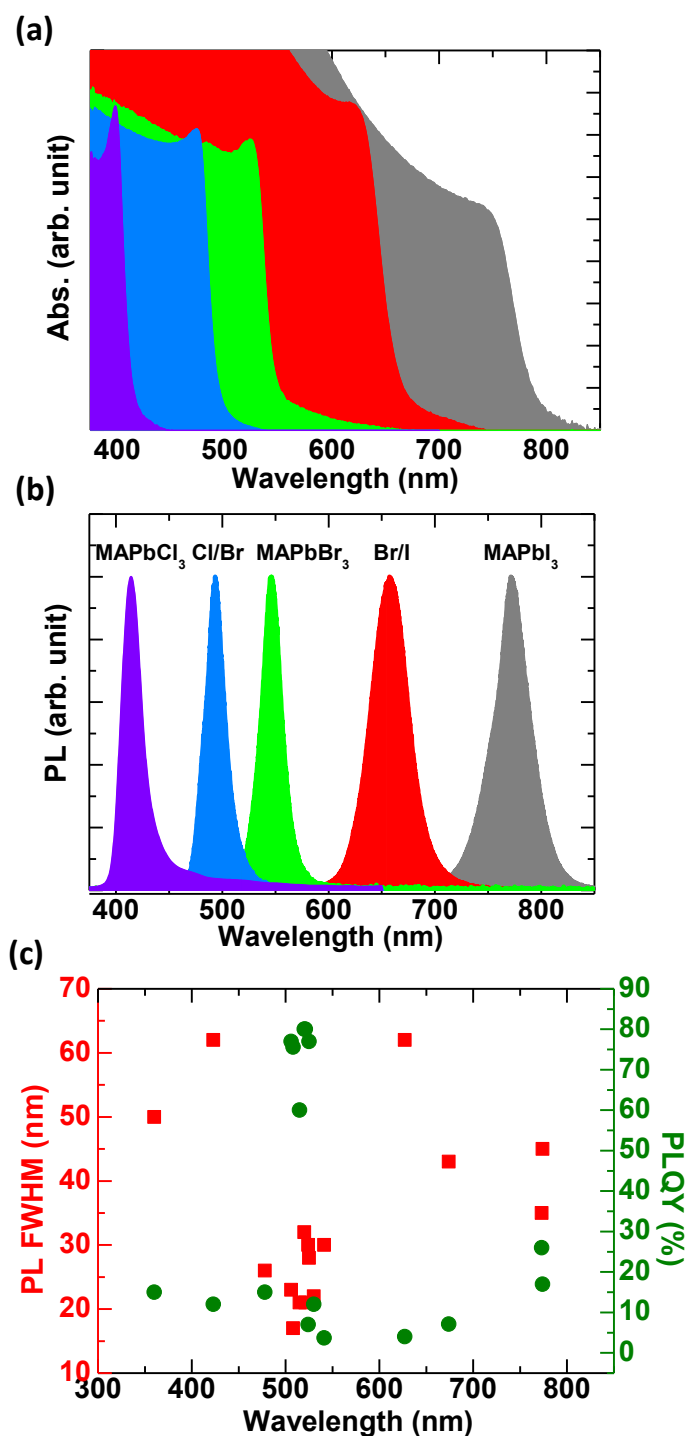


**Figure 3(a)** absorbance and **(b)** photoluminescence spectra of metal halide perovskite materials. Using the simple intermixing of halide ion, band gap can be varied from UV (410 nm) to NIR (775 nm) **(c)** Photoluminescence quantum yield (PLQY) and PL- FWHM (full width at half maxima) corresponding to different wavelengths of emitted light. In perovskite nanocrystal system, PLQY has reached 90%. [28,32,59,60,61,62,63,64,65]

Bandgap can be tuned from 1.6 eV to 2.3 eV by changing halide (I/Br) ratio <sup>[48,66]</sup> which is shown in Figure 3a and also from 2.3 eV to 3.1 eV by controlling Cl/Br ratio. <sup>[32,67]</sup> Overall, by changing the halide ratio, the band gap is tuned from 3.1eV (UV) to 1.6 eV (NIR). As the perovskite composition changes from iodine-rich to chlorine-rich, the appearance of a strong excitonic peak (just before the onset of band to band absorbance) can be observed at room temperature. The excitonic feature is more pronounced in chlorine-based perovskites. Similar excitonic features are also observed for GaAs semiconductor, although at low temperatures.<sup>[68]</sup> This is clear indication of formation of Wannier type exciton (binding energy is slightly higher than GaAs Wannier exciton, but much less than Frenkel exciton observed in organic semiconductor) with exciton binding energy lying in the range 25 to 74 meV. This large variation in binding energy is attributed to decrease in dielectric constant as the halide composition changes from I to Cl. <sup>[32,69]</sup> Thus, at room temperature ( $\approx 26$  meV) most of the Wannier-type excitons should dissociate into free charges. Hence, at room temperature one should observed a mixture of exciton and free carriers in film and as fluence power increases (to a level  $> 10^{16}$  cm<sup>-3</sup>) free carrier density dominates over exciton population density. <sup>[70]</sup> Reduction in crystal grain size also enhances the chance of finding electrons and holes within their coulomb capture radius and form stable exciton at room temperature. Below the excitonic peak, the absorption coefficient due to sub-bandgap absorption follows an exponential behavior. The slope of this exponential part is called Urbach energy and is found to lie in the range 15-50 meV for perovskites. These are low values for Urbach energy which is close to the Urbach energy of GaAs indicating the high degree of crystalline order in perovskite film.<sup>[32,33,66,71]</sup> The band gap ( $E_g$ ) of direct bandgap semiconductors is estimated using the relation,  $(\alpha E)^2 = A(E - E_g)$ , where E is the photon energy and  $\alpha$  is the measured absorption coefficient. A commonly known Tauc-plot method <sup>[72]</sup> uses a linear fit near the band-edge in the  $(\alpha E)^2$  versus energy (E) plot to determine the intercept with the energy axis and hence the

bandgap. Use of this method has been shown to yield erroneous results in the cases where excitonic features dominate the absorption spectrum.<sup>[32, 73, 74]</sup> The exciton energy levels are given by a Rydberg series,  $E_n^{ex} = E_g - R_y^*/n^2$ , where  $E_g$  is the bandgap,  $R_y^*$  the exciton Rydberg constant and  $n$  is an integer. As  $n$  increases, the exciton lines become closer in energy and at the band edge the absorption coefficient becomes large and constant instead of being zero. More accurate way of determining perovskite bandgap using Elliot or Sommerfield theory<sup>[75,76]</sup> has been elucidated by Kumawat *et. al.* along with others<sup>[77, 78]</sup> for perovskite semiconductors and using this method the bandgap was found to vary from 2.42 eV (in case of MAPbBr<sub>3</sub>) to 3.16 eV (in case of MAPbCl<sub>3</sub>) as the concentration of Cl ion ( $x$ ) varies from 0 to 1 in MAPb(Br<sub>1-x</sub>Cl<sub>x</sub>)<sub>3</sub>.<sup>[32]</sup>

### 3.2 Photoluminescence property and effect of grain size

In addition to tunable band-gap, perovskite materials demonstrates strong photoluminescent behaviour.<sup>[48,79-83]</sup> Schematic representation of photoluminescence (PL) spectra of perovskites are shown in **Figure 3b**. With varying the halide ratio (Cl/Br or I/Br), PL peak shifts accordingly following the shift in absorption edge. We have observed that under optical excitation, these materials have sharp PL peak (FWHM ~ 20-30 nm) indicating the monochromatic nature of the emission which is shown in **Figure 3c** for both organic and inorganic type perovskites, MAPbX<sub>3</sub> and CsPbX<sub>3</sub>. Photoluminescence quantum yield (PLQY) of these materials lie in the range 20-30% ( $\eta_{\text{MAPbI}_3} \sim 26\%$ ,<sup>[29]</sup>  $\eta_{\text{MAPbBr}_3} \sim 36\%$ <sup>[84]</sup>,  $\eta_{\text{MAPb(Br}_{1-x}\text{Cl}_x)_3} \sim 20\%$ <sup>[32]</sup> and  $\eta_{\text{MAPb(I}_{1-x}\text{Br}_x)_3} \sim 4\%$ <sup>[49]</sup>). These are the PLQY-values of bulk and thin film of perovskites which is rather low and considered as unsuitable for efficient LED application. However, surprisingly high PLQY  $\approx 70\%$  in MAPbI<sub>3-x</sub>Cl<sub>x</sub> system was recently reported by Deschler *et. al.*<sup>[85]</sup> at high power density levels ( $\approx 1000$  mW/cm<sup>2</sup>). In another recent breakthrough, PLQY $\sim 90\%$  was reported by Protesescu *et. al.* in an all-inorganic metal halide (CsPbX<sub>3</sub>) nanoparticle system (Figure 3c).<sup>[86]</sup>

Such high PLQY was further exploited to construct and demonstrate optically pumped laser<sup>[87,88]</sup> Therefore, despite low exciton binding energy (25-74meV) and low efficiency of exciton formation and recombination, these results suggest that the perovskites can as well be used for LED applications especially at large current densities. High level of charge carrier density increases the probability of exciton formation and helps to suppress the trap-assisted non-radiative decay channels by filling up the defect sites.

Charge carrier recombination dynamics play an important role in LED device performance.

Charge carrier recombination in semiconductors is modeled by the following equation:

$$\frac{dn(t)}{dt} = G - An(t) - Bn(t)^2 - Cn(t)^3$$

where G is the charge carrier generation rate, n(t) is the carrier concentration at time t, A, B and C are the monomolecular, bimolecular and the Auger recombination rate constants. Since exciton formation probability of perovskites are extremely low at room temperature, the first order monomolecular recombination involving geminate exciton is fairly negligible. The monomolecular recombination is largely attributed to trap assisted SRH recombination of free electron and hole. Monomolecular recombination rate for MAPbI<sub>3</sub> system was found by Herz and coworkers in the range between A = 5 × 10<sup>6</sup> and 15 × 10<sup>6</sup> s<sup>-1</sup>. However, SRH recombination probability is proportional to the trap density and hence depends on material processing and film formation methods and a wide spectrum of values for A exists in literature.<sup>[89]</sup> The non-geminate bimolecular recombination rate constant B is associated with recombination between electrons in the conduction band and holes in the valence band. Bimolecular recombination is the only radiative recombination process that dominantly contributes towards fluorescence and light emission. It has low dependency on the trap-state density hence on material processing. Yang *et al.* extracted the values of B for MAPbBr<sub>3</sub> and MAPbI<sub>3</sub> as 4.9 ± 0.2 × 10<sup>-10</sup> cm<sup>3</sup> s<sup>-1</sup> and

$1.5 \pm 0.1 \times 10^{-10} \text{ cm}^3 \text{ s}^{-1}$  respectively.<sup>[90]</sup> Herz *et. al.* has reported values at room temperature for MAPbI<sub>3</sub> in the range between  $0.6 \times 10^{-10}$  and  $9.2 \times 10^{-10} \text{ cm}^3 \text{ s}^{-1}$  which is comparable with the bimolecular recombination rate constant of  $\approx 4 \times 10^{-10} \text{ cm}^3 \text{ s}^{-1}$  for the direct-bandgap inorganic semiconductor GaAs.<sup>[89,91]</sup> Bimolecular recombination in low mobility materials are described in the framework of Langevin model, which assumes that electron and holes will recombine once they move inside the mutual coulomb capture radius. The ratio  $(B/\mu)$  (where  $\mu$  is the mobility of carriers) is estimated in Langevin theory as  $(B/\mu) = e/\varepsilon_0\varepsilon_r$  (where  $e$  is the elementary charge and the  $\varepsilon_r$  is the appropriate value of the dielectric constant). This theory has been shown to highly overestimate the value of  $B$  as compared to the value obtained in experiment. The experimental value is almost 4 orders of magnitude lower than that predicted by Langevin theory.<sup>[92]</sup> Therefore, the dominant radiative recombination mechanism in PeLEDs are quite inefficient as compared to the conjugated polymers which are predominantly excitonic emitters in nature. The luminescence observed in perovskites is primarily due to band-to-band recombination as opposed to excitonic recombination which can be understood by examining the Stokes shifts between absorption onset and photoluminescence emission peaks that are of the order of few meV for MAPbI<sub>3</sub> at room temperature.<sup>[89,93]</sup> It should be noted that, in perovskite materials, there is some fraction of excitons which remain undissociated at room temperature. These excitons also contributes to the PL and EL. The third-order Auger recombination rate becomes important at high carrier densities when an electron-hole pair recombines non-radiatively across the gap, thereby facilitating excitation of a third carrier (electron or hole) to a higher energy state. In perovskite materials  $C$  was found to be  $\approx 10^{-29} \text{ cm}^6 \text{ s}^{-1}$ . This is higher than that of GaAs ( $C \approx 10^{-30} \text{ cm}^6 \text{ s}^{-1}$ ) and CdTe ( $C \approx 0.5 \times 10^{-29} \text{ cm}^6 \text{ s}^{-1}$ ) but is of the same order of magnitude for bulk PbSe ( $C \approx 8 \times 10^{-28} \text{ cm}^6 \text{ s}^{-1}$ ).<sup>[90]</sup> This third-order process is mostly unimportant in case of LEDs, although, in lasers, this mechanism is highly relevant where a reduced Auger rate is a desired criterion.

From the preceding discussion it is evident that exciton formation probability of free carriers by moving into their joint capture radius is low and hence the bimolecular recombination rate is small in perovskites. The probability of co-capture of electron and hole can be enhanced by i) increasing the charge carrier density and ii) reducing the crystal grain size. In an interesting finding, D'Innocenzo *et al.* elucidated the dependence of luminescence properties on the crystal grain-size.<sup>[94, 95]</sup> MAPbI<sub>3</sub> grown on a flat substrate give rise to large size crystalline grains ( $\approx 500$  nm) and when infiltrated into a mesoporous oxide scaffold, grain size reduces ( $\approx 60$ -100 nm). As the grain size becomes bigger, PL lifetime increases. Transient PL data reveals a lifetime of  $\sim 2$  ns for small crystals ( $< 250$  nm), as the crystallite size grows, PL lifetime increases upto 100 ns for the largest crystallites ( $> 1$   $\mu$ m). Bimolecular radiative recombination rate was extracted from the excitation density dependent PL lifetime data and was found to be lower in case of large crystallites ( $B_{\text{rad}} = 0.62 \pm 0.06 \times 10^{-9} \text{ cm}^3 \text{ s}^{-1}$ ) than in case of smaller ones ( $B_{\text{rad}} = 3.7 \pm 0.2 \times 10^{-9} \text{ cm}^3 \text{ s}^{-1}$ ). All these results points towards the need to reduce the grain-size of perovskite crystallites in PeLEDs. The size of the crystalline grains and uniform morphology of the film depends on manifold of process-parameters such as choice of solvent, the annealing and drying conditions, concentration of precursors, deposition sequence, stoichiometric ratio of the precursors etc. A vast number of articles address this critical issue of morphology optimization for best device performance.<sup>[96]</sup> However, we confine ourselves to processing techniques that are relevant to LEDs only as focus on the recent progress in perovskite based LED research.

### 3. Perovskite Light Emitting Diodes (PeLEDs)

In case of LED, an emissive layer is sandwiched between a hole injecting and an electron injecting electrode as shown in **Figure 4(a)** and **4(b)**. A hole injection electrode/layer (HIL) is a p-type material (e.g. PEDOT:PSS, MoO<sub>3</sub>, NiO etc, **Figure 4c**) while for efficient electron

injection layer (EIL) n-type materials such as ZnO, TiO<sub>2</sub> (Figure 4c) are used. With proper work function alignment to the valance and conduction levels of the emissive materials, efficient injection of electron and hole into the emissive layer is possible, where recombination of injected charge carriers take place. In designing an efficient perovskite based LED, one important aspect is to optimize perovskite processing conditions in order to achieve high quality, pin-hole free, crystalline film on top of substrates. For fabrication purpose, two different device configurations are adapted (see figure 4(a) and 4(b)). In one case, the so called p-i-n configuration, LED is built on top of p-type hole injecting electrode (PEDOT:PSS) and the n-type material is a fullerene derivative (PC<sub>61</sub>BM), while in the other, it is built atop an n-type electron injection electrode (ZnO or TiO<sub>2</sub>) and the configuration is called n-i-p. The p-type layer is a hole transport material such as a deep HOMO p-type semiconductor (for a more complete list, see Figure 4c). In both the cases, a transparent substrate (glass/indium or fluorine doped tin oxide (ITO or FTO) enables the light to come out from the device. The choice of the configuration is sometimes driven by the fact that perovskite film growth and crystallinity depends on the surface energy of the underlying layer.

Perovskite surface morphology is an important issue for the success of the light emitting devices. Particularly for LED devices, one needs pin-hole free perovskite layer which is also having low surface roughness value to prevent shunting pathway in devices. This is one of the reason, most of the PeLED devices are made on PEDOT:PSS rather than on TiO<sub>2</sub> or ZnO and mesoporous Al<sub>2</sub>O<sub>3</sub> scaffolds. Planar compact TiO<sub>2</sub> layer was used very successfully for growing large size crystalline domains. As the crystallinity increases, the surface roughness also increases.<sup>[97]</sup> On top of PEDOT:PSS, on the other hand, perovskite film is more amorphous and comprised of small sized crystalline grains. This rather amorphous but compact layer of perovskite offers low surface roughness. Surface energy of the underlying layer plays a major role in initiation of nucleation and growth of perovskite material. A

hydrophilic surface like PEDOT:PSS offers better wettability and thus faster nucleation which ultimately leads to small grain-sized crystals and uniform film.<sup>[98]</sup> In **Figure 5a-5d**, we have summarized the number of publications reporting a p-i-n configuration and those reporting an n-i-p configuration. Clearly, p-i-n configuration has been more preferred and successful geometry for PeLEDs. Organic-inorganic and inorganic PeLEDs EQE for green, red, orange and blue emission are shown by **Figure 5e & 5f**. In the report on LED operating at room temperature by Tan *et al.*, 3D- perovskite materials MAPbI<sub>3-x</sub>Cl<sub>x</sub>, MAPbBr<sub>3</sub> and MAPbBr<sub>2</sub>I was used to demonstrate infrared, green and red color emission, respectively. The device configuration for MAPbI<sub>3-x</sub>Cl<sub>x</sub> device was n-i-p type where, perovskite layer was spin coated on top of n-type TiO<sub>2</sub> layer. Due to poor coverage of perovskite material atop TiO<sub>2</sub>, the device configuration was changed to p-i-n type diode, ITO/PEDOT:PSS/MAPbBr<sub>3</sub>/F8/Ca/Ag and bright green EL with luminance of 364 cd/m<sup>2</sup> was observed.<sup>[29]</sup> Coverage on PEDOT:PSS is substantially better as compared to TiO<sub>2</sub> or ZnO, however, PEDOT:PSS poses certain limitations that are detrimental to device efficiency. At the PEDOT:PSS-MAPbBr<sub>3</sub> perovskite interface, there exist injection barrier for hole (~ 0.8 eV). In addition, quenching of excitons take place at the interface, contributing to the losses. Therefore interlayer is used to prevent the quenching and improve charge injection in PeLED. Following this approach Kim *et al.* improved the efficiency by using a perfluorinated polymeric acid, tetrafluoroethylene-perfluoro-3,6-dioxa-4-methyl-7-octene-sulfonic acid copolymer (PFI) layer in between PEDOT:PSS/MAPbBr<sub>3</sub> interface and achieved 417 cd/m<sup>2</sup> in glass/ITO/PEDOT:PSS/PFI/MAPbBr<sub>3</sub>/1,3,5-tris(1-phenyl-1H-benzimidazol-2-yl)benzene(TPBi)/LiF/Al diode.<sup>[99]</sup> This "self-organized" PFI layer prevents exciton from quenching at the interface and removes hole injection barrier by modifying the work-function of PEDOT:PSS, at the same time it makes PEDOT:PSS more electron blocking. Meanwhile, Hoye *et al.* used spatial atmospheric atomic layer-deposited (SAALD) ZnO as a electron

injection layer with Mg doping in ITO/PEDOT:PSS/MAPbBr<sub>3</sub>/ZnO (or Mg doped ZnO)/Ca/Ag configuration and achieved luminance of 550 cd/m<sup>2</sup> with very low turn-on voltage of 2V. In this device structure electron injection barrier was reduced and the hole blocking was enhanced by doping ZnO with Mg.<sup>[100]</sup> Surface modification of ZnO with high electron affinity material is an useful and well known technique to enhance the electron injection/collection by modifying its work function by means of surface dipole moments.<sup>[101,102]</sup> Recently, this concept was utilized by Wang *et. al.* who modified ZnO with polyethylenimine (PEI) in ITO/ZnO/PEI/MAPbBr<sub>3</sub>/TFB/MoO<sub>3</sub>/Au device structure and reported luminance of 20,000 cd/m<sup>2</sup>. This device gave an EQE of 0.8%, corresponding IQE of 3.6% and 4 lm/W power efficiency.<sup>[103]</sup> Furthermore, PEI layer was shown to promote high quality pin-hole free perovskite film formation with high degree of crystallinity. A similar approach was adopted by Yu *et. al.* who used a thin layer of a polar-solvent, ethanolamine (EA) on top of compact TiO<sub>2</sub> (c-TiO<sub>2</sub>) as a modifier of TiO<sub>2</sub> work-function and the surface-energy.<sup>[104]</sup> The electron injection barrier was lowered by 0.3 eV and as a result, green color LED with luminance of 544 cd/m<sup>2</sup> at 5.8V was reported with the device configuration, ITO/c-TiO<sub>2</sub>/EA/MAPbBr<sub>3</sub>/SPB-02T/MoO<sub>3</sub>/Au. Based on the similar strategy Wang *et. al.* used amino-acid based self assembled monolayer on top of ZnO layer to demonstrate EQE ~ 0.43% and brightness of 5000 cd/m<sup>2</sup> in MAPbBr<sub>3</sub> based LED.<sup>[105]</sup> Thus, the usage of interlayer can boost the performance of the device in three different ways, by reducing the injection barrier, suppressing the exciton quenching at the interface and promoting a uniform pin-hole free perovskite film growth.

Due to the low binding energy, in perovskite material excitons are readily dissociated at room temperature leading to quenching of the luminescence. In order to enhance the probability of free electron and free hole capture and their subsequent bimolecular radiative recombination, it is therefore required to confine the charge carriers within the emissive layer. In order to construct such a "well" it is therefore required to sandwich the perovskite layer between two

electrodes which will inject one type of charge carrier efficiently and block the other. Tan *et al.* used TiO<sub>2</sub> and poly(9,9'-dioctylfluorene)(F8) combination. F8 by virtue of its large bandgap with deep HOMO level and shallow LUMO, it allows holes to inject and confine them in the perovskite layer while it blocks electron efficiently.<sup>[29]</sup> Several other researchers,<sup>[106, 107]</sup> including Kumawat *et al.*<sup>[49]</sup> used N,N'-bis(3-methylphenyl)-N,N'-diphenylbenzidine (TPD) to efficiently block electrons and confine holes in the emissive layer. Alternatively, the confinement of free carriers can be achieved via reduction in the thickness of the emissive perovskite layer and reduction in crystal grain size.<sup>[29,84]</sup> Tan *et al.* used only 15 nm thick perovskite layer to limit the free carrier diffusion length and thereby forcing electron-hole capture and recombination.<sup>[29]</sup> Reduction in grain size and increase in grain-boundary region facilitates the spatial confinement of exciton and charge carriers by preventing their diffusion and thereby increases the radiative recombination.<sup>[84]</sup> These requirements are completely opposite for solar cells where larger grain sizes are required in order to promote free carrier generation.<sup>[108]</sup>

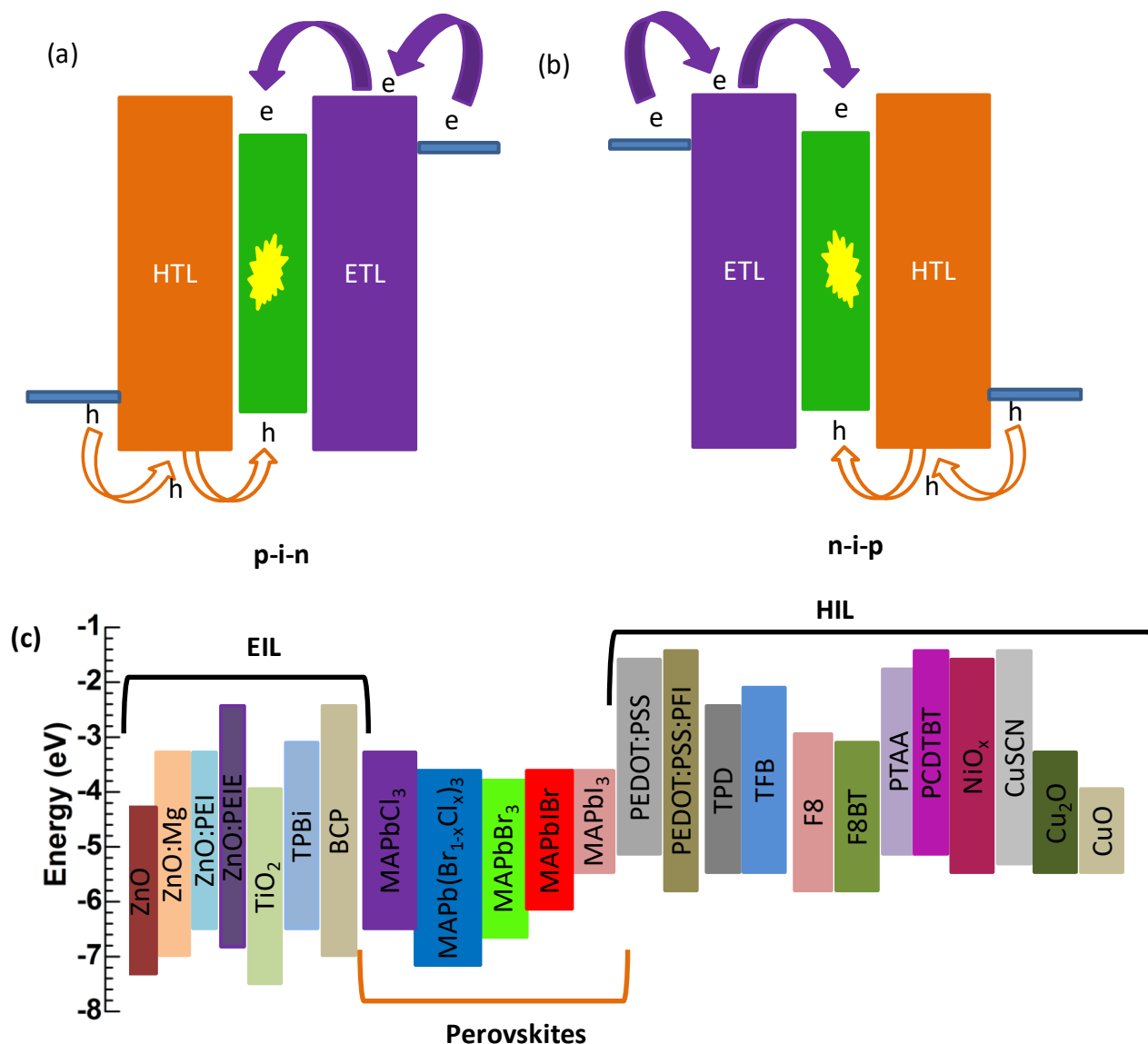


**Figure 4** Standard PeLED device configurations: (a) p-i-n (b) n-i-p (c) Energy level diagram of perovskite with hole and electron injection layers for better charge carrier injection balance in PeLEDs where energy level values of HOMO and LUMO has been taken from literature.

[84,109,110,111,112,113]

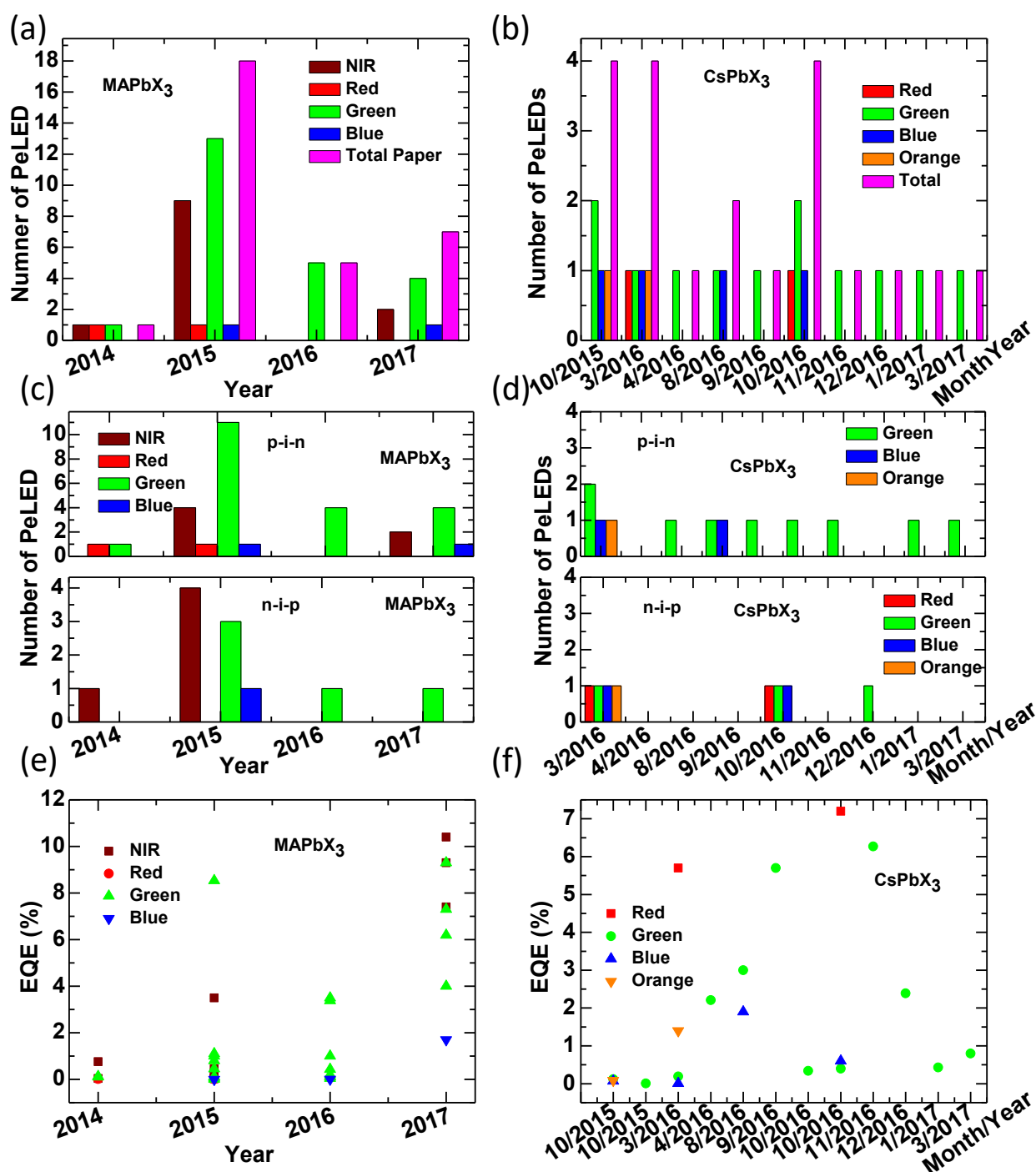


**Figure 5** Number of PeLEDs using (a) MAPbX<sub>3</sub> and (b) CsPbX<sub>3</sub> perovskite materials as emissive layer. Reports on green LEDs are more in number as compared to orange, red, blue and orange LEDs. (c) & (d) Number of reports on PeLED in two configuration p-i-n and n-i-p and our data suggests that p-i-n configuration is more favorable for PeLED than n-i-p for both types of perovskites (MAPbX<sub>3</sub> and CsPbX<sub>3</sub>). (e) & (f) EQE of PeLEDs having NIR, red, green, orange and blue emissive perovskites along with the year of reporting for organic-inorganic (MAPbX<sub>3</sub>) [29,32,33,49,59,60,61,84,99,100,104,105].

114 , 115 , 116 , 117 , 118 , 119 , 120 , 121 , 122 , 123 , 124 ] and inorganic (CsPbX<sub>3</sub>) PeLEDs. [65, 125 , 126 , 127,128,129,130,131,132,133,134,135,136]

In order to achieve film uniformity in perovskite film and reduce the grain size, anti-solvent treatment is used frequently. Rapid crystallization of perovskite using an anti-solvent is perhaps the most effective technique to obtain uniform pin-hole free layer with large surface coverage. [84,137] In this technique, an solvent (such as toluene, chlorobenzene, benzene, p-xylene, chloroform etc.) which is a bad solvent or anti-solvent for the perovskite precursor but completely miscible with the host solvent in which perovskite precursors are dissolved (such as DMSO, DMF, GBL etc.) is introduced by direct dripping on the film during spin coating. Presence of the anti-solvent reduces the solubility of the perovskite precursors, forcing the rapid precipitation of the precursor components and at the same time good solvent DMSO and DMF, mixed with the anti-solvent is removed by spinning off and gives the high nucleation rate. [84] Removal of DMSO is crucial since a slow evaporation of DMSO prevents the rapid reaction between perovskite precursors by forming DMSO-lead halide complexes. By adding anti-solvent, supersaturation condition is achieved much faster and hence nucleation of perovskite crystals is initiated rapidly. Jeon *et al.* used toluene as an anti-solvent [138] whereas chlorobenzene was chosen as anti-solvent by Xiao *et al.* [139] Cho *et al.* used nanocrystal pinning (solvent-based NCP or S-NCP) technique where, an low boiling point anti-solvent chloroform is used. [84] Chloroform evaporates faster and thus removes DMSO at a faster rate forcing rapid crystallization. Additionally, Cho *et al.* used a small molecule 2,2',2''-(1,3,5-benzinetriyl)-tris (1-phenyl-1-H-benzimidazole) (TPBi) as an additive to chloroform (additive-based NCP or A-NCP) to further reduce growth of crystal and reducing the grain size. By limiting the MAPbBr<sub>3</sub> grain size to an average diameter of 99 nm and optimizing the methylammonium bromide (MABr) concentration in the MAPbBr<sub>3</sub> solution, luminance of 10000 cd/m<sup>2</sup> at 7.5 V was achieved with EQE of 8.53%. [84]

In contrast, there is an opposite approach where an acid (such as HBr and HI) is used to achieve the supersaturation state at the later stage of spin coating promoting a thinner layer with high surface coverage of perovskite. Heo *et al.* demonstrated this technique by mixing controlled amount of HBr in DMF.<sup>[140]</sup> As the solubility parameter increases, during the spin coating process, perovskite nucleation starts at a much later stage when DMF+HBr has evaporated to some extent and concentration of perovskite in the wet film has reached supersaturation point. Since this happens over longer time scale, the thickness of the spinning film reduces and hence a compact film of perovskite is obtained. Adapting a similar technique, Yu *et al.* optimized the device using MAPbBr<sub>3</sub> perovskite material and DMF/HBr solvent combination (6 vol% HBr in DMF) that yielded maximum luminance of 3490 cd/m<sup>2</sup> and luminous efficiency of 0.43 cd/A (at 4.3 V).<sup>[117,141]</sup>

Precursor stoichiometry, is another key parameter that affects the final film morphology to a great extent. In the initial stages of development of this field, MAI (methylammonium iodide) and PbI<sub>2</sub> (lead iodide) was mixed in equal molar ratio (1:1) in  $\gamma$ -butyrolacetone solvent and resultant solution was spun on mesoporous TiO<sub>2</sub> substrates. Later, it was found that, a non-stoichiometric mixture of MAI:PbCl<sub>2</sub> in the ratio 3:1, greatly increases the quality of the crystalline film as compared to the pure halide based perovskites (MAPbI<sub>3</sub> or MAPbBr<sub>3</sub>).<sup>[142]</sup> Mixed halide perovskite of type MAPbI<sub>3-x</sub>Cl<sub>x</sub> and MAPb(I<sub>1-x</sub>Br<sub>x</sub>)<sub>3</sub> has been extensively studied by Kumawat *et al.* for light emitting applications.<sup>[32,49]</sup> Among the mixed halide perovskite films deposited on PEDOT:PSS substrate, MAPbI<sub>3-x</sub>Cl<sub>x</sub> had much bigger crystalline domain size as compared to MAPbBr<sub>3</sub> and MAPbI<sub>3-x</sub>Br<sub>x</sub>. The large Urbach energy in MAPbI<sub>3-x</sub>Br<sub>x</sub> also indicated the large disorder present in these films. A somewhat similar finding was reported by Sadhalana *et al.* where, changing the Br content in MAPbI<sub>3-x</sub>Br<sub>x</sub>, increased the disorder in the film and a high Urbach energy of 90 meV was found for MAPbI<sub>0.6</sub>Br<sub>2.4</sub>.<sup>[66]</sup> However, changing the chlorine molar concentration in MAPb(Br<sub>1-x</sub>Cl<sub>x</sub>)<sub>3</sub> type mixed halide, from x=0 (MAPbBr<sub>3</sub>) to

$x = 3$  ( $\text{MAPbCl}_3$ ), it was found that the Urbach energy does not change significantly. Incorporation of chlorine therefore does not introduce any structural disorder, however, the grain size of the film was seen to vary.<sup>[32]</sup> Effect of stoichiometry was further explored by Cho *et al.* By controlling the  $\text{MABr}$  and  $\text{PbBr}_2$  ratio, they tried to minimize the Pb content in the film.<sup>[84]</sup> Metallic lead clusters act as non-radiative recombination site which exists throughout the bulk of the crystal as was confirmed by XPS studies.<sup>[84,143]</sup> To reduce the lead content, the ratio of  $\text{MABr}$  and  $\text{PbBr}_2$  was varied ( $\text{MABr}:\text{PbBr}_2 = 1.05:1, 1:1$  and  $1:1.05$ ). In addition to that, nanocrystal pinning (NCP) method (as described before) was used. The resultant film was uniform and comprised of small size crystals of 150-200 nm average crystallite size (see in **Figure 6a & 6b** for device structure and device performance).

PeLED fabrication is also done via vacuum deposition processes. In vacuum deposition process, both the precursors are either co-evaporated<sup>[144]</sup> or evaporated sequentially, where the deposition of  $\text{PbX}_2$  was preceded by deposition of  $\text{MAX}$ .<sup>[145]</sup> In hybrid type of process, the lead halide film is deposited by spin-coating and subsequently it is exposed to methylammonium halide vapour<sup>[146]</sup> or dipped into the solution containing methylammonium halide.<sup>[147]</sup> Gil-Escrig *et al.* reported LED devices fabricated via a combination of co-evaporation and hybrid deposition technique.<sup>[107]</sup> First a layer of  $\text{MAPbI}_3$  was deposited by co-evaporation of precursors ( $\text{MAI}$  and  $\text{PbI}_2$ ). On top of this layer a single layer of  $\text{PbBr}_2$  was evaporated which was subsequently converted to  $\text{MAPbBr}_3$  layer by exposure to  $\text{MABr}$  solution via spin coating.

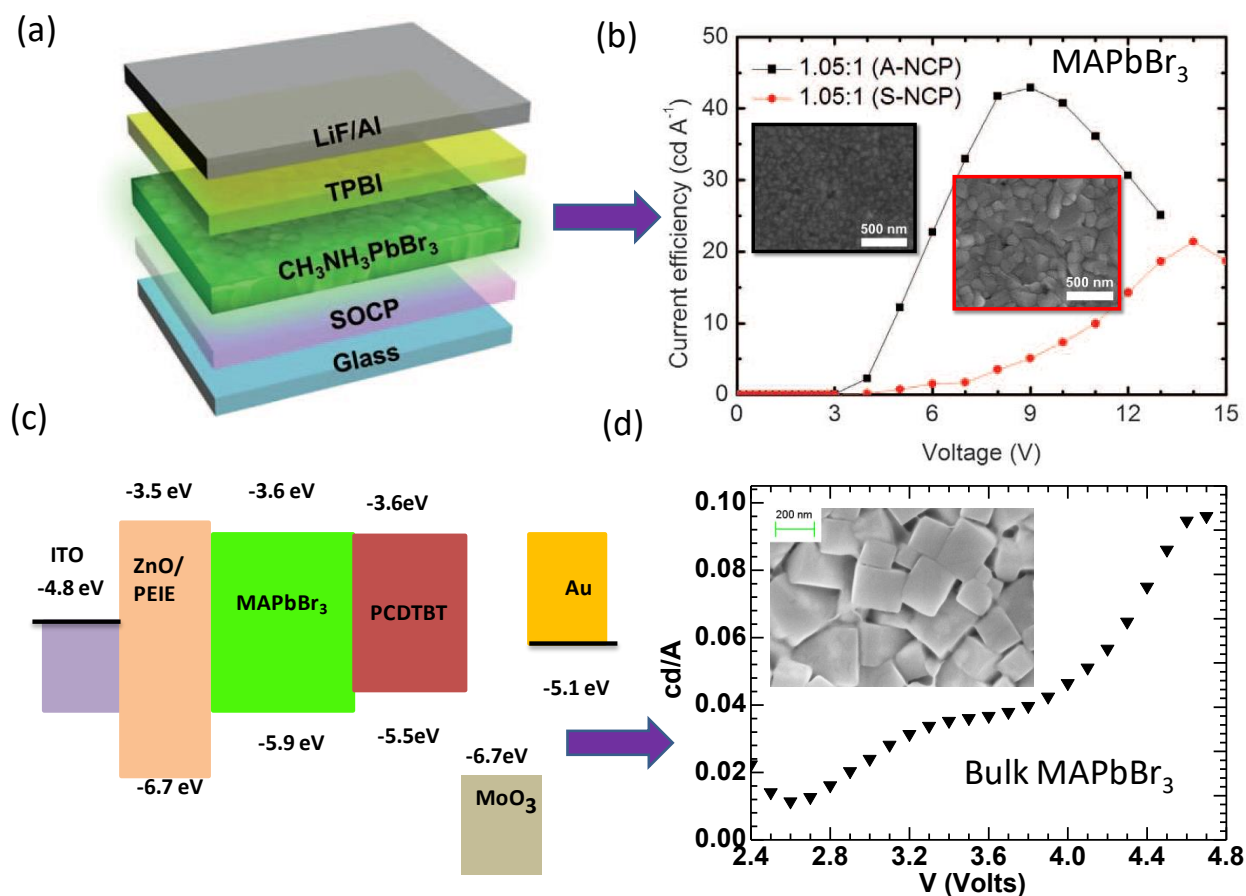


**Figure 6** (a) Schematic diagram of PeLED and (b) corresponding current efficiency (cd/A) versus applied voltage characteristics corresponding to different grain-sizes (shown in the inset).<sup>[84]</sup> Figure 6a and 6b suggest that optimized molar ratio and reduced grain size can result in high PeLED performance. (c) Schematic flat energy level diagram and (d) corresponding current efficiency (cd/A) versus applied voltage characteristics for ITO/ZnO/PEIE/MAPbBr<sub>3</sub>/PCDTBT/MoO<sub>3</sub>/Au device (n-i-p configuration) with optimized molar ratio of MABr (0.27M) and PbBr<sub>2</sub> (1.5M). Inset of figure shows the FESEM image of MAPbBr<sub>3</sub> on ZnO/PEIE substrate.<sup>[148]</sup>

This bilayer structure of MAPbI<sub>3</sub> and MAPbBr<sub>3</sub> was annealed to form a hybrid perovskite MAPb(I<sub>1-x</sub>Br<sub>x</sub>)<sub>3</sub>. LED devices were fabricated in p-i-n geometry atop a ITO/ PEDOT:PSS/poly-TPD layer, albeit low EQE value of ~ 0.06%. Kumawat *et. al.* has demonstrated MAPbBr<sub>3</sub> thin

film deposition via sequential deposition technique with optimized molar ratio of MABr and  $\text{PbBr}_2$  ( $\text{MABr}:\text{PbBr}_2 = 0.27\text{M}:1.5\text{M}$ ). First a layer of  $\text{PbBr}_2$  is spin coated on substrate, subsequently a layer of MABr is spin coated atop  $\text{PbBr}_2$  thin film. This technique resulted in a compact morphology for PeLEDs and a current efficiency of  $0.1\text{cd/A}$  was achieved using ITO/ZnO/PEIE/MAPbBr<sub>3</sub>/PCDTBT/MoO<sub>3</sub>/Au device configuration (shown in Figure 6(c) and Figure 6(d)). FESEM image of spin coated sequentially deposited MAPbBr<sub>3</sub> thin film reveals an average grain size of 300nm (Figure 6d inset).<sup>[148]</sup> Optimization of molar ratio of MABr and  $\text{PbBr}_2$  in conjunction with reduction in grain-size is, therefore, a promising approach towards high efficiency PeLED.<sup>[84,148]</sup>

Although, bulk perovskite film based LED technology has shown great promise, the highest reported EQE of 10.4% is still much below than that of quantum dot based LED ( $\approx 20\%$ ) and organic LED ( $\approx 30\%$ ).<sup>[30,31,149, 150]</sup> The large grain size (100-500 nm) of the bulk-phase perovskite is definitely a roadblock to achieve high quantum efficiency. Several processing techniques like anti-solvent treatment, acidic treatment, sequential deposition, vacuum evaporation give rise to huge variation in the resultant film morphology and consequently introduces defect states that can quench PL via non-radiative SRH recombination.<sup>[84]</sup> It is proposed that trap sites that quench the PL in these materials are situated not only at the surface but also in the interior (bulk) of the crystals, the later being more difficult to deactivate via background illumination. Hence one has to use high fluence or apply large bias voltage to achieve large carrier density ( $> 10^{16}\text{ cm}^{-3}$ ) which will fill up the deep trap states and increase radiative recombination.<sup>[70]</sup> In small sized crystallites or nanoparticles of perovskites, subbandgap defect states due to bulk trap states are much lower and it is easier to deactivate surface trap states by chemical passivation. Although, one should note, if not passivated properly, nanoparticles have high density of trap states ( $\sim 10^{18}\text{ cm}^{-3}$  for 10 nm MAPbBr<sub>3</sub> as compared to  $\sim 10^9\text{ cm}^{-3}$  for large millimeter sized MAPbBr<sub>3</sub> crystal) due to increased surface to

volume ratio.<sup>[70, 151, 152]</sup> Strong exciton confinement due to small size effect (particle diameter  $\leq$  exciton Bohr diameter) in case of perovskite nanoparticles also contributes to the bright PL with reported PLQY value reaching upto 90% from a modest 20% as in the case of bulk phase thin films.<sup>[32,84,59-65]</sup>

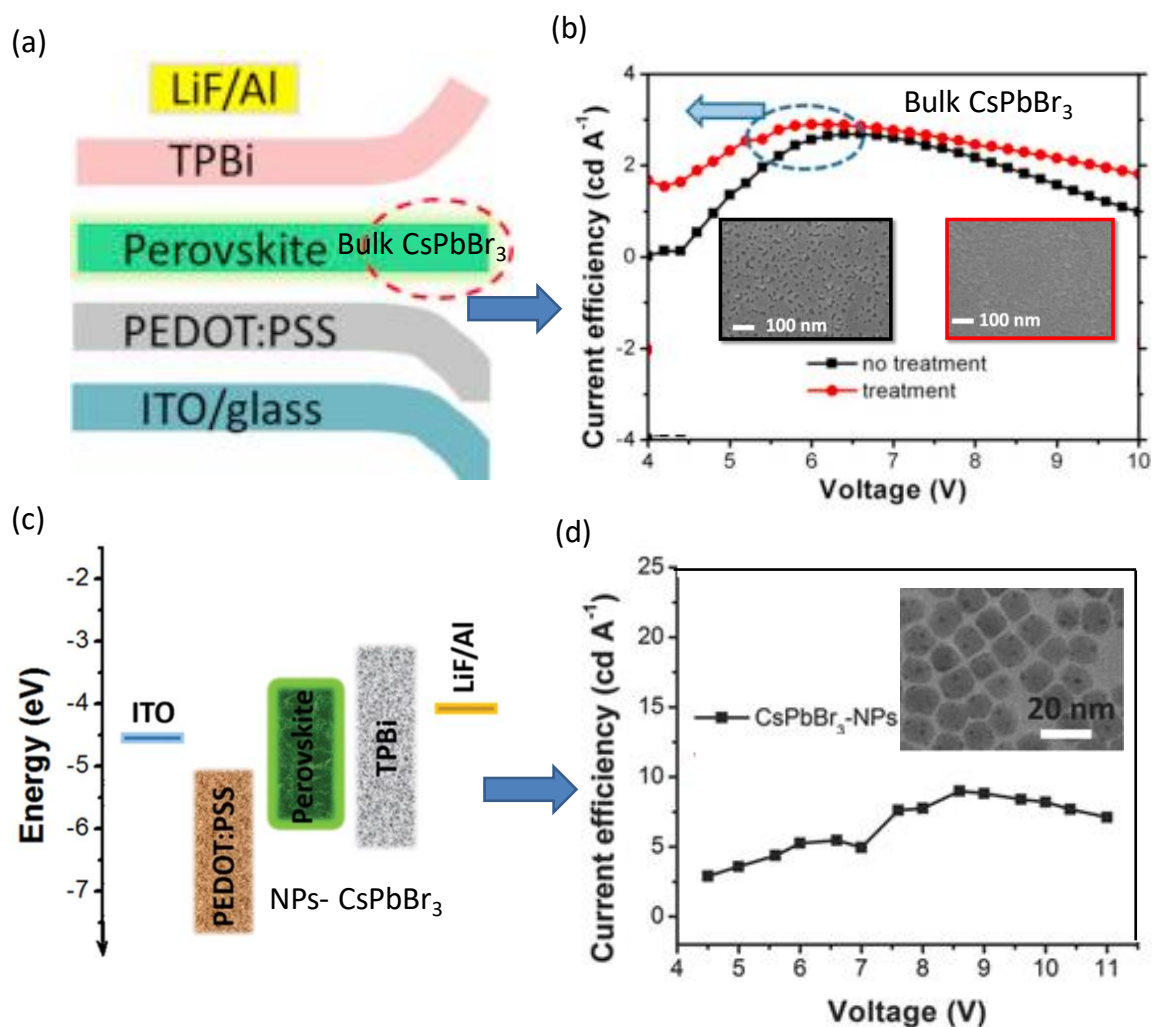


**Figure 7** (a) Schematic diagram of inorganic PeLED device structure and (b) corresponding current efficiency (cd/A) versus applied voltage characteristics for ITO/PEDOT:PSS/CsPbBr<sub>3</sub>/TPBi/LiF/Al device. Inset of the figure is the FESEM image of bulk CsPbBr<sub>3</sub> thin film with anti-solvent treatment<sup>[132]</sup> (c) Flat energy level diagram of CsPbBr<sub>3</sub> nanoparticle-based PeLED and (d) corresponding current efficiency (cd/A) versus applied

voltage characteristics. TEM image of the nanoparticles is shown in the inset.<sup>[128]</sup> Nanoparticles of inorganic PeLEDs also yield improved performance over the bulk-phase.

Synthesis techniques of nano-particles include two major approaches, namely, hot-injection technique<sup>[86]</sup> and addition of precursor solution in a good solvent (e.g. DMF) to a bad solvent (e.g. Toluene) followed by stabilizing with ligands (e.g. oleic acid and oleylamine).<sup>[128-136]</sup>

Although the high PLQY is obtained in solution of nanoparticles, it is often difficult to obtain high EL in devices. It is mainly because of the fact that PLQY drops to some extent upon formation of film. This drop can be attributed to increased surface states that promotes non-radiative recombination.<sup>[128 -139]</sup> Furthermore, using nano particles, pin-hole free thin film is difficult to achieve. Li *et al.* in Cavendish Lab circumvented this problem by embedding perovskite nano-particles in an insulating polyimide precursor (PIP) matrix. Using a p-i-n type configuration, ITO/PEDOT:PSS/MAPbBr<sub>3</sub>:PIP/F8/Ca/Ag this group reported EQE of 1.2% and luminance of 200 cd/m<sup>2</sup> at current density of 3.1 mA/cm<sup>2</sup>.<sup>[114]</sup> An improvement over this approach was obtained by using an ionic conductive polymer, poly(ethylene oxide) (PEO)-perovskite composite emissive layer and a luminance of 4064 cd/m<sup>2</sup> was reported.<sup>[116]</sup> For the green emitting MAPbBr<sub>3</sub>, best demonstrated EQE and luminance of 0.48% and 10590 cd/m<sup>2</sup> was achieved by Ling *et al.* via synthesis of nanosized perovskite platelets.<sup>[60,123]</sup> Using these nanoplatelets in conjunction with a capping layer of charge transporting polymers (poly(9-vinylcarbazole) (PVK) and 2-(4-biphenyl)-5-phenyl-1,3,4-oxadiazole) (PBD), Ling *et al.* reported green light emission with luminance of 10590 cd/m<sup>2</sup> at 12V. PVK and PBD polymers were blended together in an optimized ratio and was spin coated on top of perovskite to reduced the surface roughness of film and improve the charge injection balance in the device. Apart from the nanoplatelets, LED based on MAPbBr<sub>3</sub> quantum dots (with size ~ 10 nm), has been demonstrated in p-i-n configuration ITO/PEDOT:PSS/MAPbBr<sub>3</sub>/TPBi/CsF/Al, and EQE of 1.1% and luminance of 2503 cd/m<sup>2</sup> was reported.<sup>[59]</sup> So far, there are only few reports on the

successful demonstration of the methylammonium (MA) cation based perovskites nanoparticle LED. Difficulty to obtain pin-hole free layer and large amount of surface defect states are the major roadblock to achieve higher efficiency numbers.

Poor thermal stability of MAPbX<sub>3</sub> type perovskites is also a major concern that reduces the operational lifetime of the LED. At high current densities, self-heating effect may lead to the disintegration of the perovskite. In some of the recent studies it has been shown that an optimized thermal annealing procedure can be beneficial for the stability.<sup>[59,120,121]</sup> A more successful and well accepted approach to circumvent this problem is to replace the MA cation with Cs cation.<sup>[153]</sup> CsPbBr<sub>3</sub> shows much higher evaporation/decomposition onset (~ 650 °C) as compared to MAPbBr<sub>3</sub> (~ 220 °C).<sup>[154]</sup> A very high PLQY (~ 90%) with high degree of colour purity (12 ≤ FWHM ≤ 42 nm) and wide range of color tunability (410-700 nm) for these all inorganic (CsPbX<sub>3</sub>: X= Cl, Br, I) perovskite nanoparticles (~ 4-15 nm in size) has been reported by Protesescu *et. al.*<sup>[86]</sup> Using nano-particles of CsPbCl<sub>3-x</sub>Br<sub>x</sub> for blue emission, CsPbBr<sub>3</sub> for green emission and CsPbI<sub>3-x</sub>Br<sub>x</sub> for red emission, Song *et. al.* reported LED devices with EQE of 0.07%, 0.12% and 0.09% for blue, green and red LED respectively.<sup>[125]</sup> A big improvement in the EQE values was achieved by Li *et. al.*<sup>[127]</sup> who used a cross linking method to freeze the nanoparticles in the film and by stopping it from dissolving in any solvent. The nanoparticle film was exposed to controlled amount of trimethylaluminium (TMA) vapor that created a hydroxide-terminated aluminum oxide network among the nano-particles. Due to the cross-linking, nano-particle layer becomes completely insoluble allowing the deposition of a hole-injecting (and electron blocking) polymer layer via spin coating. With this technique a remarkably high EQE of 5.7% was achieved for the CsPbI<sub>3</sub>-nanoparticle based red emitting LED. Similar EQE value for green color emission has been reported very recently by Yu and his team, where they used CsPbBr<sub>3</sub>, poly-(ethylene oxide) (PEO), and poly(vinylpyrrolidone) (PVP) composite emissive layer without any additional EIL and HIL.<sup>[134]</sup> Zhang *et. al.*

incorporated a layer of Ag nanowires on top of PEDOT:PSS and demonstrated an enhanced EQE of 0.43% for green emitting CsPbBr<sub>3</sub> nanoparticle based LEDs.<sup>[135]</sup> The performance of inorganic bulk-phase PeLEDs are much inferior than nanoparticle-based PeLEDs (shown in **Figure 7**). Current efficiency (cd/A) of inorganic nanoparticle PeLEDs are three times higher than that of bulk-phase.<sup>[128,132]</sup>

The present state of the art LEDs based on nanoparticles with EQE and luminance values 5.7% and 206 cd/m<sup>2</sup><sup>[34]</sup> for red emission, 0.48%, 10590 cd/m<sup>2</sup><sup>[125]</sup>, 1.1%, 2503 cd/m<sup>2</sup><sup>[60]</sup> and 5.7%, 591197 cd/m<sup>2</sup><sup>[134]</sup> for green emission, are still much below than that of their competing technologies, namely, organic(O)-LED and quantum dot (QD)-LED. However, the progress has been very rapid in this field which took only two years of intense research to reach this level since the first report in 2014.<sup>[29]</sup> Nevertheless, few challenges such as appropriate passivation of surface defect states using ligands, integrity and quality of the pin hole free layer, overcoming the electrical injection barrier due to the presence of the ligands, are still remaining for the efficiency numbers to improve and become competitive.

#### 4. Challenges and Future Directions

The "Perovskite Phenomenon" has come up as a hugely promising technology for light harvesting as well as light generation within a brief span of time. Mixed halide based perovskites, emitting visible colors (blue, green and red) are the front runner materials to make LEDs. At this exciting stage of development, the technology is facing several challenges. Poor reproducibility of film morphology due to lack of a single robust processing technique, poor thermal and environmental stability, toxicity issue due to the presence of Pb metal are some of the long-term challenges that has to be addressed for industrial viability. Our immediate research goal, on the other hand, should be concentrated on improving the device performance. One major part of the EL is lost due to poor out-coupling in these devices.

Perovskites have relatively higher refractive index ( $n_{\text{pero}} \sim 2.0$ ) as compared to the organic polymers ( $n_{\text{organic}} \sim 1.7$ ) and glass substrates ( $n_{\text{glass}} \sim 1.5$ ) which leads to light trapping due to total internal reflections within the device. In order to improve out-coupling there are photonic solutions available in the form of index grids <sup>[155]</sup>, micro-lenses <sup>[156]</sup> and patterning of substrates.<sup>[157]</sup> Separately tackling these three efficiency parameters can easily give a substantial boost in existing out-coupling efficiency numbers, which is close to 5.7% ( $\eta_{\text{oc}}$ ) at present for bulk MAPbBr<sub>3</sub> based PeLEDs.<sup>[148]</sup> Optimal, balanced charge carrier injection into the emissive layer requires smooth and pin-hole free interfaces between perovskite emitter and the electron or hole transport layers. Nano-composite of 3D perovskites in organic matrix seems to provide a solution for this where combination of host material vs guest perovskite needs to be selected wisely by looking at electronic states so that charge transfer processes do not take place and it forms type-I heterostructure. A reduction in leakage current, i.e. enhancement in charge carrier injection balance factor can easily boost the efficiency further. Another future direction to boost the performance for PeLEDs is to optimize the material properties to enhance absolute PL efficiency, as being reported recently by making quasi-2D perovskites using these 3D wide bandgap perovskite semiconductors.<sup>[158,159]</sup> By substituting the MA cation with larger organic ammonium cation, such as, phenylethyl ammonium (PEA), perovskite crystal structure changes to a 2D layered structure. Consequently the exciton becomes more confined and the binding energy increases upto 200 meV. Optimizing the 2D-perovskite (PEA)<sub>2</sub>PbBr<sub>4</sub> and 3D-perovskite MAPbBr<sub>3</sub> ratio, high efficiency green LED was realized.<sup>[159]</sup> Based on such quasi 2D-perovskite structure (PEA<sub>2</sub>(MA)<sub>n-1</sub>Pb<sub>n</sub>I<sub>3n+1</sub>) infrared LED was also reported recently with EQE = 8.8%.<sup>[158]</sup> However, the efficiency values in these 2D-perovskite based LEDs are restricted by poor mobility of charge carriers, primarily due to the presence of insulating organic-ammonium groups. Nano-particles of perovskites on the other hand has come in the forefront with large PLQY value approaching 100% and high colour

purity. Despite this fact, only a few successful cases of nano-particle based LEDs has been reported. Although the presence of capping ligands are essential for controlling the grain-growth and hence limiting the particle size, for prevention of the aggregation and also for passivating surface trap states, these insulating ligands seems to pose a problem for efficient injection of charge carriers. Furthermore, the large difference between the PLQY in solution and in thin film of these nanoparticles needs to be addressed.<sup>[160]</sup> Very recently Pan et. al. demonstrated a significant progress in efficiency of all inorganic perovskite ( $\text{CsPbX}_3$ ) nanoparticle based LEDs by replacing the long ligands (such as oleylamine and oleic acid) with shorter ligands (such as di-dodecyl dimethyl ammonium bromide) and thereby achieving a maximum EQE and luminance of 3.0% and  $330 \text{ cd m}^{-2}$  respectively.<sup>[136]</sup>

While the device efficiency is maturing to a competitive level, some of the challenges such as viability for large area fabrication, thermal and moisture stability of perovskites and toxicity issue due to presence of Pb has to be met with long-term solution. Depending on the processing techniques there is a large variability in the morphology of the thin films. Therefore it is challenging to obtain uniform pin hole free film over large area by employing large-area compatible printing technique. Recently, a fully-printed PeLED fabricated in ambient atmosphere has been demonstrated on flexible substrate with EQE  $\sim 1.1\%$  and luminance of  $21014 \text{ cd m}^{-2}$ .<sup>[118]</sup> Perovskites are unstable under exposure to moisture and tends to decompose. The stability issue has been discussed in some of the recent reviews.<sup>[161, 162]</sup> By substituting MA cation with FA (formamidinium) cation or Cs cation can improve the stability.<sup>[163]</sup> However, perovskite based on FA cations have much inferior charge carrier mobility which restricts the device performance. Hence to circumvent this problem a more intense research is required on right type of charge injection layers and the morphology of the perovskite. Toxicity problem due to presence of Pb is one more challenge for this technology. Some of the recent report has addressed this issue and argued that Pb contamination to the

environment due to exposure to moisture is either below the hazardous limit<sup>[164]</sup> or can be handled in an efficient manner.<sup>[165]</sup> Alternatively, by replacing Pb with more environmentally benign material like Sn, promising PLQY values has been obtained, although, no EL has been reported till date. The main stumbling block is the creation of p-type defects due to oxidation of  $\text{Sn}^{2+}$  to  $\text{Sn}^{4+}$  which quenches the luminescence.<sup>[166, 167]</sup> Perovskites are also unstable under electrical stress which is attributed to the ion-migration in some of the 3D perovskites. Under prolong operation of the LEDs, the perovskite material may decompose and degrade and thus can become unsuitable for the long lifetime of the LEDs. Such ionic migration has been addressed by using appropriate charge injection and blocking layer and also by using pulsed electrical bias in conjunction with constant background voltage.<sup>[29]</sup> A constant background voltage of appropriate polarity helps to drive out the ionic traps from bulk emissive layer which otherwise would act as mediator for non-radiative recombination. Once these ions are moved away towards the contacts, the device is polarized and radiative recombination is enhanced. Hence the EQE is higher in a pre-polarized PeLED as compared to a unpolarized one.

## 5. Conclusions

Metal halide perovskite semiconductor are not only successful for photovoltaic technology but it has potential to be successful material for future lighting and display technology, thanks to its high quantum yield, colour-tunability over large range, narrow PL emission and consequent colour purity and low material cost. Low exciton binding energy is a drawback which can be tackled via quantum confinement in nano sized particles and using 2D layered perovskites. Within very short interval of time, the efficiency of PeLEDs has improved to a great extent but still the physics of these materials is not very well understood. Apart from electrical and environmental stability issues, the device efficiency, particularly for red and blue emitting perovskite is far below than its green emitting counterpart. It is evident that nano sized

perovskites holds the maximum promise for future of this technology. Therefore, the exciton dynamics and non-radiative recombination arising due to surface defect states has to be well understood. With intense focus on the remaining challenges and adopting to the research approaches towards the right direction, it is only a matter of time to obtain the efficiency level comparable to inorganic LEDs. Observing the success of the photovoltaic devices, a bright future for organic-inorganic halide based perovskites for application in LEDs can therefore be envisioned.

### Acknowledgements

This work is partially supported by the Department of Science & Technology (DST/TM/SERI/FR/186(G)), India. We also acknowledge support of Centre of Excellence in Nanoelectronics (CEN) for deposition facility and National Centre for Photovoltaic Research and Education (NCPRE) for characterization. We thank Prof. Anil Kumar from Chem. IITB-Mumbai for providing synthesis facility

**Table 1** Performance parameters of perovskite light emitting diodes (PeLEDs) with different device structure (n-i-p and p-i-n) with different perovskite emissive layers.

p-i-n device structure based PeLEDs			
Perovskite PeLED	cd/A	EQE	Refs.
ITO/PEDOT:PSS/MAPbBr <sub>3</sub> /F8/Ca/Ag	0.3	0.1	29
ITO/PEDOT:PSS/MAPbBr <sub>2</sub> /F8/Ca/Ag	0.03	0.018	29
ITO/PEDOT:PSS:PFI/MAPbBr <sub>3</sub> /TPBi/LiF/Al	0.577	0.125	99
ITO/PEDT:PSS/MAPbI <sub>3-x</sub> Cl <sub>x</sub> /PCBM/Ag	-	0.18	49
ITO/PEDT:PSS/TPD/MAPbBr <sub>2</sub> /Ag	-	0.0065	49
ITO/PEDT:PSS/TPD/MAPbBr <sub>3</sub> /Ag	-	0.0011	49
ITO/PEDT:PSS/MAPbI <sub>3-x</sub> Cl <sub>x</sub> Br <sub>y</sub> /PCBM/Ag	-	0.28	49

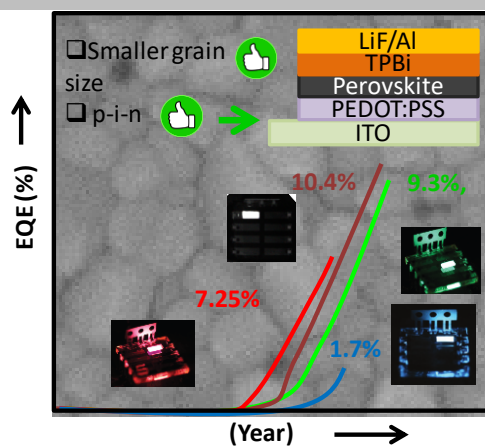
ITO/PEDOT:PSS/MAPbBr <sub>3</sub> :PIP/F8/Ca/Ag	-	1.2	114
ITO/PEDOT:PSS/MAPbBr <sub>3</sub> /TmPyPB/LiF/Al	-	0.1	115
ITO/PEDOT:PSS/MAPbBrCl/PCBM/Ag	3E-4	2E-4	32
ITO/PEDOT:PSS/TPD/MAPbIBr/PCBM/Ba/Ag	-	0.02	107
ITO/PEDOT:PSS/MAPbBr <sub>3</sub> /SPB-02T/LiF/Ag	0.43	0.10	117
ITO/PEDOT:PSS/PVK:PBD/MAPbBr <sub>3</sub> /BCP/LiF/Al	-	0.48	123
ITO/PEDOT:PSS:PFI/MAPbBr <sub>3</sub> /TPBi/LiF/Al	42.9	8.53	84
ITO/PEDOT:PSS/MAPbBr <sub>3</sub> -QDs/TPBi/CsF/Al	4.5	1.1	60
ITO/PEDOT:PSS/MAPbBr <sub>3</sub> /SPW-111/LiF/Al	0.92	0.20	104
ITO/PEDOT:PSS/MAPbBr <sub>3</sub> /TPBi/LiF/Al	0.577	0.125	121
ITO/PEDOT:PSS/TPD/MAPbBr <sub>3</sub> NPs/TPBi/Cs <sub>2</sub> Co <sub>3</sub> /Al	11.49	3.8	124
ITO/PEDOT:PSS/MAPbBr <sub>3</sub> /TPBi/LiF/Al	8.22	-	59
ITO/PEDOT:PSS/CsPbBr <sub>3</sub> -NPs/TPBi/LiF/Al	8.98	2.21	128
ITO/PEDOT:PSS/CsPbBr <sub>3</sub> /F8/Ca/Ag	0.008	0.03	126
ITO/PEDOT:PSS:PVK/CsPbBr <sub>3</sub> -NC/TPBi/LiF/Ag	1.15	0.34	129
ITO/PEDOT:PSS:PVK/CsPbBrCl-QDs/TPBi/LiF/Al	0.14	0.07	125
ITO/PEDOT:PSS:PVK/CsPbBr <sub>3</sub> -QDs/TPBi/LiF/Al	0.43	0.12	125
ITO/PEDOT:PSS:PVK/CsPbIBr-QDs/TPBi/LiF/Al	0.08	0.09	125
ITO/PEDOT:PSS/p-TPD/CsPbBr <sub>3</sub> -QDs/TPBi/LiF/Al	13.3	6.27	133
ITO/PEDOT:PSS/CsPbBr <sub>3</sub> /TPBi/LiF/Al	2.90	0.9	132
	0.19	0.06	131
ITO/NiO/MAPbBr <sub>3</sub> /TPBi/LiF/Al	15.9	-	168
ITO/p-TPD/MAPbI <sub>3</sub> /TPBi/LiF/Al	0.09	10.4	30
ITO/PVK/MAPbBr <sub>3</sub> /TPBi/LiF/Al	17.1	9.3	30
ITO/PEDOT:PSS/MAPbBr <sub>3</sub> /TmPyPB/LiF/Al	15.26	3.38	169
ITO/PEDOT:PSS/TCTA/PEO:MAPbBr <sub>3</sub> /TmPyPB/CsF/Al	15.1	4	170
ITO/PEDOT:PSS/MAPbBr <sub>3</sub> -QD/TPBi/CsF/Al	3.72	1.06	122
ITO/PEDOT:PSS/MAPbBr <sub>3</sub> /TPBi/LiF/Al	8.22	-	59
ITO/PEDOT:PSS/MAPbBr <sub>3</sub> /APMs/SPW-111/LiF/Ag	28.9	6.19	141
ITO/p-TPD/MAPbI <sub>3</sub> /TPBi/LiF/Al	-	7.4	171
<b>n-i-p device structure based PeLEDs</b>			
ITO/TiO <sub>2</sub> /MAPbI <sub>3-x</sub> Cl <sub>x</sub> /F8/MoO <sub>3</sub> /Ag	-	0.76	29
ITO/TiO <sub>2</sub> /MAPbI <sub>3-x</sub> Cl <sub>x</sub> /Spiro/MoO <sub>3</sub> /Au	-	0.024	172
ITO/ZnO/PEI/MAPbI <sub>3-x</sub> Cl <sub>x</sub> /TFB/MoO <sub>3</sub> /Au	-	3.5	103
ITO/ZnO/PEI/MAPbBr <sub>3</sub> /TFB/MoO <sub>3</sub> /Au	-	0.8	103
FTO/TiO <sub>2</sub> /MAPbI <sub>3-x</sub> Cl <sub>x</sub> /Spiro/Au	-	0.48	173
ITO/c-TiO <sub>2</sub> /MAPbBr <sub>3</sub> /SPB-02T/MoO <sub>3</sub> /Au	0.11	0.026	104
ITO/c-TiO <sub>2</sub> /EA/MAPbBr <sub>3</sub> /SPB 02T/MoO <sub>3</sub> /Au	0.22	0.051	104
ITO/ZnO/MAPbBr <sub>3</sub> /Al <sub>2</sub> O <sub>3</sub> /PEDOT:PSS/Au	0.12	0.064	119

ITO/ZnO/5AVA+CB/MAPbBr <sub>3</sub> /TFB/MoO <sub>3</sub> /Au		0.43	105
ITO/ZnO/PEIE/MAPbBr <sub>3</sub> /PCDTBT/MoO <sub>3</sub> /Au	0.10	0.023	148
FTO/c-TiO <sub>2</sub> /mp-TiO <sub>2</sub> /MAPbBr <sub>3</sub> /P3HT/Au	0.0034	1.4E-5	174
ITO/ZnO/PEI/MAPbBr/1-NCs/CBP/TCTA/MoO <sub>3</sub> /Au	0.49	7.25	130
c-Al <sub>2</sub> O <sub>3</sub> /n-GaN/n-MgZnOCsPbBr <sub>3</sub> -QDs/p-MgNiO/Au	2.25	2.39	65
ITO/ZnO/CsPbI <sub>3</sub> -QDs/TFB/MoO <sub>3</sub> /Ag	-	5.7	34
ITO/ZnO/CsPbI <sub>2.25</sub> Br <sub>0.75</sub> -QDs/TFB/MoO <sub>3</sub> /Ag	-	1.4	34
ITO/ZnO/CsPbBr <sub>3</sub> -QDs/TFB/MoO <sub>3</sub> /Ag	-	0.19	34
ITO/ZnO/CsPbCl <sub>1.5</sub> Br <sub>1.5</sub> -QDs/TFB/MoO <sub>3</sub> /Ag	-	0.0074	34
ITO/ZnO/PVP/CsMAPbBr <sub>3</sub> /CBP/MoO <sub>3</sub> /Al	33.9	10.4	31

Layout 1:

## REVIEW

Perovskite light emitting device performance depends grain size and device architecture. In this review we report current status of PeLED research.



Dinesh Kabra\*

Page No.1 – Page No.49

Recent Advancement in  
Metal Halide Based  
Perovskite Light  
Emitting Diodes

Accepted Manuscript

**References:**

- [1] W. Faschingera, J. Nurnberger, *Appl. Phys. Lett.* **2000**, 77, 2000.
- [2] H. J. A. Round, *Electrical World* **1907**, 19, 309.
- [3] O. Graydon, *Nature Photonics* **2010**, doi:10.1038/nmat2656.
- [4] O. V. Lossev, *Philosophical Magazine, Series* **1928**, 75, 1024–1044
- [5] R. Braunstein, *Physical Review* **1955**, 99, 1892.
- [6] J. R. Biard, G. E. Pittman, Semiconductor Radiant Diode US3293513 A
- [7] N. Holonyak, S. F. Bevacqua, *Appl. Phys. Lett.* **1962**, 1, 82.
- [8] S. Nakamura, T. Mukai, M. Senoh, *Appl. Phys. Lett.* **1994**, 64, 1687.
- [9] Y. Jiang, Y. Li, Y. Li, Z. Deng, T. Lu, Z. Ma, P. Zuo, L. Dai, L. Wang, H. Jia, W. Wang, J. Zhou, W. Liu, H. Chen, *Sci. Rep.* **2015**, 5, 10883. (DOI: 10.1038/srep10883)
- [10] S. Nakamura, T. Mukai, M. Senoh, *Japanese J. App. Phys.* **1991**, 22, 1998-2001.
- [11] S. Jha, J.-C. Qian, O. Kutsay, J. K. Jr, C.-Y. Luan, J. A. Zapien, W. Zhang, S.-T. Lee, I. Bello, *Nanotechnology* **2011**, 22, 245202.
- [12] A. Bernanose, M. Comte, P. Vouaux, *J. Chim. Phys.* **1953**, 50, 64.
- [13] A. Bernanose, P. Vouaux, *J. Chim. Phys.* **1953**, 50, 261.
- [14] A. Bernanose, *J. Chim. Phys.* **1955**, 52, 396.
- [15] H. Kallmann, M. Pope, *J. Chem. Phys.* **1960**, 32, 300.
- [16] C. W. Tang, S. A. Vanslyke, *Appl. Phys. Lett.* **1987**, 51, 913.
- [17] J. H. Burroughes, D. D. C. Bradley, A. R. Brown, R. N. Marks, K. MacKay, R. H. Friend, P. L. Burns, A. B. Holmes, *Nature* **1990**, 347, 539-541.
- [18] X. Yang, X. Xu, G. Zhou, *J. Mater. Chem. C* **2015**, 3, 913.
- [19] [http://www.nrel.gov/ncpv/images/efficiency\\_chart.jpg](http://www.nrel.gov/ncpv/images/efficiency_chart.jpg).

- [20] S. De Wolf, J. Holovsky, S.-J. Moon, P. Loper, B. Niesen, M. Ledinsky, F.-J. Haug, J.-H. Yum, C. Ballif, *J. Phys. Chem. Lett.* **2014**, *5*, 1035-1039.
- [21] S. D. Stranks, G. E. Eperon, G. Grancini, C. Menelaou, M. J. P. Alcocer, T. Leijtens, L. M. Herz, A. Petrozza, H. J. Snaith, *Science* **2013**, *342*, 341-344.
- [22] T. Leijtens, S. D. Stranks, G. E. Eperon, R. Lindblad, E. M. J. Johansson, I. J. McPherson, H. Rensmo, J. M. Ball, M. M. Lee, H. J. Snaith, *ACS Nano*, **2014**, *8*, 7147–7155
- [23] N. Kitazawa, Y. Watanabe, Y. Nakamura, *J. Mater. Sci.* **2002**, *37*, 3585-3587.
- [24] K. Tvingstedt, O. Malinkiewicz, A. Baumann, C. Deibel, H. J. Snaith, V. Dyakonov, H. J. Bolink, *Nat. Sci. Rep.* **2014**, *4*, 1.
- [25] M. Era, S. Morimoto, T. Tsutsui, S. Saito, *Appl. Phys. Lett.* **1994**, *65*, 676–678.
- [26] T. Hattori, T. Taira, M. Era, T. Tsutsui, S. Saito, *Chem. Phys. Lett.* **1996**, *254*, 103–108.
- [27] K. Chondroudis, D. B. Mitzi, *Chem. Mater.* **1999**, *11*, 3028–3030.
- [28] L. Schmidt, A. Pertegas, S. Gonzalez-Carrero, O. Malinkiewicz, S. Agouram, G. M. Espallargas, H. J. Bolink, R. E. Galian, J. Perez- Prieto *J. Am. Chem. Soc.* **2014**, *136*, 850–853.
- [29] Z.-K. Tan, R. S. Moghaddam, M. L. Lai, P. Docampo, R. Higler, D. Felix, M. Price, A. Sadhanala, L. M. Pazos, D. Credgington, F. Hanusch, T. Bein, H. J. Snaith, R. H. Friend, *Nat. Nanotechnology* **2014**, *9*, 687-692.
- [30] Z. Xiao, R. A. Kerner, L. Zhao, N. L. Tran, K. M. Lee, T.-W. Koh, G. D. Scholes, B. P. Rand, *Nature Photonics* **2017**, *11*, 108.
- [31] L. Zhang, X. Yang, Q. Jiang, P. Wang, Z. Yin, X. Zhang, H. Tan, Y. (Michael) Yang, M. Wei, B. R. Sutherland, E. H. Sargent, J. You, *Nature Communication* **2017**, *8*, 15640.
- [32] N. K. Kumawat, A. Dey, K. L. Narshimhan, D. Kabra, *ACS App. Mat. & Interfaces* **2015**, *7*, 13119.

- [33] A. Sadhanala, S. Ahmad, B. Zhao, N. Giesbrecht, P. M. Pearce, F. Deschler, R. L. Z. Hoye, K. C. Godel, T. Bein, P. Docampo, S. E. Dutton, M. F. L. De Volder, R. H. Friend, *Nano Lett.* **2015**, *15*, 6095.
- [34] G. Li, F. W. R. Rivarola, N. J. L. K. Davis, S. Bai, T. C. Jellicoe, F. de la Pena, S. Hou, C. Ducati, F. Gao, R. H. Friend, N. C. Greenham, Zhi-Kuang Tan, *Adv. Mater.* **2016**, *28*, 3528.
- [35] S. Pathak, N. Sakai, F. W. R. Rivarola, S. D. Stranks, J. Liu, G. E. Eperon, C. Ducati, K. Wojciechowski, J. T. Griffiths, A. A. Haghighirad, A. Pellaroque, R. H. Friend, H. J. Snaith, *Chem. Mater.* **2015**, *27*, 8066.
- [36] M. Helen, *Nature* **1945**, *155*, 484.
- [37] T. C. Sum, N. Mathews, *Energy Environ. Sci.* **2014**, *7*, 2518.
- [38] S. D. Stranks, H. J. Snaith, *Nature Nanotechnology* **2015**, *10*, 391–402.
- [39] G. Nedelcu, L. Protesescu, S. Yakunin, M. I. Bodnarchuk, M. J. Grotevent, M. V. Kovalenko, *Nano Lett.* **2015**, *15*, 5635.
- [40] V. M. Goldschmidt, *Ber. Dtsch. Chem. Ges.* **1927**, *60*, 1263–1268.
- [41] M. Johnsson, P. Lemmens, *Advanced Magnetic Materials, John Wiley & Sons, Ltd.* **2007**.
- [42] C. Li, X. Lu, W. Ding, L. Feng, Y. Gao, Z. Guo, *Acta Crystallogr. Sect. B: Struct. Sci.* **2008**, *B64*, 702.
- [43] P. Hagemuller, Chemistry and Physics; Eds.; Materials Science Series; *Academic Press*: London, **1985**.
- [44] Q. Chen, N. De Marco, Y. Yang, T.-B. Song, C.-C. Chen, H. Zhao, Z. Hong, H. Zhou, Y. Yang, *Nano Today* **2015**, *10*, 355.
- [45] R. D. Shannon, *Acta Crystallogr. A* **1976**, *A32*, 751-767
- [46] N.-G. Park, *Materials Today*, **2015**, *18*, 65.
- [47] A. Kumar, N. K. Kumawat, P. Maheshwari, D. Kabra, *Photovoltaic Specialist Conference (PVSC) IEEE 42nd* **2015** (DOI:10.1109/PVSC.2015.7355732).

- [48] J. H. Noh, S. H. Im, J. H. Heo, T. N. Mandal, S. Il Seok, *Nano Lett.* **2013**, *13*, 1764.
- [49] N. K. Kumawat, A. Dey, K. L. Narshimhan, D. Kabra, *ACS Photonics* **2015**, *2*, 349-354.
- [50] A. Kojima, K. Teshima, Y. Shirai, T. Miyasaka, *J. Am. Chem. Soc.* **2009**, *131*, 6050.
- [51] Y. H. Chang, C. H. Park, *Journal of the Korean Physical Society* **2004**, *44*, 889.
- [52] N. Onoda-Yamamuro, T. Matsuo, H. Suga, *J. Phys. Chem. Solids* **1990**, *51*, 1383-1395.
- [53] C. M. Sutter-Fella Y. Li, M. Amani, J. W. Ager, F. M. Toma, E. Yablonovitch, I. D. Sharp, A. Javey, *Nano Lett.*, **2016**, *16*, 800–806.
- [54] B. G. Sreetman, S.-K. Banerjee, Solid State Electronic Devices 6th Edition ISBN 013149726X, **2005**.
- [55] H. Yu, F. Wang, F. Xie, W. Li, J. Chen, N. Zhao, *Adv. Funct. Mater.* **2014**, *24*, 7102.
- [56] G. Xing, N. Mathews, S. Sun, S. S. Lim, Y. M. Lam, M. Gratzel, S. Mhaisalkar, T. C. Sum, *Science* **2013**, *342*, 344.
- [57] A. M. A. Leguy, P. Azarhoosh, M. I. Alonso, M. Campoy-Quiles, O. J. Weber, J. Yao, D. Bryant, M. T. Weller, J. Nelson, A. Walsh, M. V. Schilfgaard, P. R. F. Barnes, *Nanoscale* **2016**, *8*, 6317.
- [58] N. K. Kumawat, M. N. Tripathi, U. Waghmare, D. Kabra, *J. Phys. Chem. A* **2016**, *120*, 3917.
- [59] J. Liang, Y. Zhang, X. Guo, Z. Gan, J. Lin, Y. Fana, X. Liu, *RSC Adv.* **2016**, *6*, 71070.
- [60] H. Huang, F. Zhao, L. Liu, F. Zhang, X.-G Wu, L. Shi, B. Zou, Q. Pei, H. Zhong, *ACS Appl. Mater. Interfaces* **2015**, *7*, 28128.
- [61] F. Zhang, H. Zhong, C. Chen, X.-gang Wu, X. Hu, H. Huang, J. Han, B. Zou, Y. Dong, *ACS Nano* **2015**, *9*, 4533.
- [62] L. Peng, A. Tang, C. Yang, F. Teng, *J. Alloys and Compounds*, 2016, 687, 506.
- [63] M. Leng, Z. Chen, Y. Yang, Z. Li, K. Zeng, K. Li, G. Niu, Y. He, Q. Zhou, J. Tang, *Angew. Chem.* **2016**, *128*, 1 – 6.

- [64] C. Guhrenz, A. Benad, C. Ziegler, D. Haubold, N. Gaponik, A. Eychmuller, *Chem. Mater.* **2016**, 28, 9033.
- [65] Z. Shi, Y. Li, Y. Zhang, Y. Chen, X. Li, D. Wu, T. Xu, C. Shan, G. Du, *Nano Lett.* **2017**, 17, 313.
- [66] A. Sadhanala, F. Deschler, T.-H. Thomas, S. E. Dutton, K. C. Goedel, F. C. Hanusch, M. L. Lai, U. Steiner, T. Bein, P. Docampo, D. Cahen, R. H. Friend, *J. Phys. Chem. Lett.* **2014**, 5, 2501.
- [67] R. Comin, G. Walters, E. S. Thibau, O. Voznyy, Z.-H. Lub, E. H. Sargent, *J. Mater. Chem. C* **2015**, 3, 8839.
- [68] R. P. Seisyan, V. A. Kosobukin, S. A. Vaganov, G. N. Aliev, O. S. Coschug, *Proc. SPIE* 1985, Physical Concepts and Materials for Novel Optoelectronic Device Applications II, **1993**, 794.(doi:10.1117/12.162811)
- [69] K. Tanakaa, T. Takahashia, T. Bana, T. Kondoa, K. Uchidab, N. Miura, *Solid State Communications* **2003**, 127, 619.
- [70] S. D. Stranks, V. M. Burlakov, T. Leijtens, J. M. Ball, A. Goriely, H. J. Snaith, *Phys. Rev. Appl.*, **2014**, 2, 034007.
- [71] S. De Wolf, J. Holovsky, S.-J. Moon, P. Loper, B. Niesen, M. Ledinsky, F.-J. Haug, J.-H. Yum, C. Ballif, *J. Phys. Chem. Lett.* **2014**, 5, 1035.
- [72] T. M. Koh, K. Fu, Y. Fang, S. Chen, T. C. Sum, N. Mathews, S. G. Mhaisalkar, P. P. Boix, T. Baikie, *J. Phys. Chem. C* **2014**, 118, 16458.
- [73] S. L. Chuang, *Physics of Optoelectronics Devices*, 1st ed.; Wiley: New York, **1995**.
- [74] M. A. Green, Y. Jiang, A. M. Soufiani, A. Ho-Baillie, *J. Phys. Chem. Lett.* **2015**, 6, 4774.
- [75] R. J. Elliott, *Phys.Rev.* **1957**, 108, 1384.
- [76] A. Mukherjee, S. Ghosh, *J. Appl. Phys.* **2014**, 115, 123503.

- [77] P. Kumar, C. Muthu, V. C. Nair, K. S. Narayan, K. S. Narayan, *J. Phys. Chem. C*, **2016**, *120*, 18333–18339
- [78] M. Saba, M. Cadelano, D. Marongiu, F. Chen, V. Sarritzu, N. Sestu, C. Figus, M. Aresti, R. Piras, A. G. Lehmann, C. Cannas, A. Musinu, F. Quochi, A. Mura, G. Bongiovanni, *Nat. Commun.* **2014**, *5*, 5049
- [79] D. M. Jang, K. Park, D. H. Kim, J. Park, F. Shojaei, H. S. Kang, J.-P. Ahn, J. W. Lee, J. K. Song, *Nano Lett.* **2015**, *15*, 5191.
- [80] P. Tyagi, S. M. Arveson, W. A. Tisdale, *J. Phys. Chem. Lett.* **2015**, *6*, 1911.
- [81] L. C. Schmidt, A. Pertegast, S. Gonzalez-Carrero, O. Malinkiewicz, S. Agouram, G. M. Espallargas, H. Bolink, R. E. Galian, J. Perez-Prieto, *J. Am. Chem. Soc.* **2014**, *136*, 850-853.
- [82] N. K. Noel, A. Abate, S. D. Stranks, E. S. Parrott, V. M. Burlakov, A. Goriely, H. J. Snaith, *ACS Nano* **2014**, *8*, 9815.
- [83] P. Kumar, C. Muthu, V. C. Nair, K. S. Narayan, *J. Phys. Chem. C*, **2016**, *120*, 18333.
- [84] H. Cho, S.-H. Jeong, M.-H. Park, Y.-H. Kim, C. Wolf, C.-L. Lee, J. H. Heo, A. Sadhanala, N. Myoung, S. Yoo, S. H. Im, R. H. Friend, T.-W. Lee, *Science* **2015**, *350*, 1222.
- [85] F. Deschler, P. Michael, S. Pathak, L. E. Klintberg, D.-D. Jarausch, R. Higler, S. Hüttner, S.; T. Leijtens, S. D. Stranks, H. J. Snaith, M. Atature, R. T. Phillips, R. H. Friend, *J. Phys. Chem. Lett.* **2014**, *5*, 1421.
- [86] L. Protesescu, S. Yakunin, M. I. Bodnarchuk, F. Krieg, R. Caputo, C. H. Hendon, R. X. Yang, A. Walsh, M. V. Kovalenko, *Nano Lett.* **2015**, *15*, 3692.
- [87] G. Xing, N. Mathews, S. S. Lim, N. Yantara, X. Liu, D. Sabba, M. Gratzel, S. Mhaisalkar, T. C. Sum, *Nature Materials*, **2014**, *13*, 476.
- [88] H. Zhu, Y. Fu, F. Meng, X. Wu, Z. Gong, Q. Ding, M. V. Gustafsson, M. T. Trinh, S. Jin, X.-Y. Zhu, *Nature Materials* **2015**, *14*, 636.
- [89] M. B. Johnston, L. M. Herz, *Acc. Chem. Res.* **2016**, *49*, 146–154.

- [90] Y. Yang, M. Yang, Z. Li, R. Crisp, K. Zhu, M. C. Beard, *J. Phys. Chem. Lett.* **2015**, *6*, 4688.
- [91] M. Sheik-Bahae, R. I. Epstein, *Phys. Rev. Lett.* **2004**, *92*, 247403.
- [92] C. Wehrenfennig, G. E. Eperon, M. B. Johnston, H. J. Snaith, L. M. Herz, *Adv. Mater.* **2014**, *26*, 1584–1589.
- [93] R. L. Milot, G. E. Eperon, H. J. Snaith, M. B. Johnston, L. M. Herz, *Adv. Funct. Mater.* **2015**, *25*, 6218–6227.
- [94] G. Grancini, S. Marras, M. Prato, C. Giannini, C. Quarti, F. D. Angelis, M. D. Bastiani, G. E. Eperon, H. J. Snaith, L. Manna, A. Petrozza, *J. Phys. Chem. Lett.* **2014**, *5*, 3836.
- [95] V. D’Innocenzo, A. R. S. Kandada, M. D. Bastiani, M. Gandini, A. Petrozza, *J. Am. Chem. Soc.* **2014**, *136*, 17730.
- [96] N. J. Jeon, J. H. Noh, Y. C. Kim, W. S. Yang, S. Ryu, S. Il Seok, *Nature Materials* **2014**, *13*, 897.
- [97] X. Ren, Z. Yang, D. Yang, X. Zhang, D. Cui, Y. Liu, Q. Wei, H. Fan, S. Liu, *Nanoscale* **2016**, *8*, 3816.
- [98] T. Salim, S. Sun, Y. Abe, A. Krishna, A. C. Grimsdale, Y. M. Lam, *J. Mater. Chem. A* **2015**, *3*, 8943.
- [99] Y. H. Kim, H. Cho, J. H. Heo, T.-S. Kim, N. Myoung, C.-L. Lee, S. H. Im, T.-W. Lee, *Adv. Mater.* **2015**, *27*, 1248.
- [100] R. L. Z. Hoyer, M. R. Chua, K. P. Musselman, G. Li, M.-L. Lai, Z.-K. Tan, N. C. Greenham, J. L. MacManus-Driscoll, R. H. Friend, D. Credgington, *Adv. Mater.* **2015**, *27*, 1414–1419.
- [101] B. R. Lee, H. Choi, J. S. Park, H. J. Lee, S. O. Kim, J. Y. Kim, M. H. Song, *J. Mater. Chem.* **2011**, *21*, 2051.
- [102] Y. Vaynzof, T. J. Dennes, J. Schwartz, A. Kahn, *Appl. Phys. Lett.* **2008**, *93*, 103305.

- [103] J. Wang , N. Wang , Y. Jin, J. Si , Z.-K. Tan, H. Du, L. Cheng, X. Dai , S. Bai , H. He, Z. Ye, M. L. Lai , R. H. Friend, W. Huang, *Adv. Mater.* **2015**, 27, 2311.
- [104] J. C. Yu, D. B. Kim, G. Baek, B. R. Lee, E. D. Jung, S. Lee, J. H. Chu , D.-K. Lee, K. J. Choi, S. Cho, M. H. Song, *Adv. Mater.* **2015**, 27, 3492.
- [105] N. Wang, L. Cheng, J. Si, X. Liang, Y. Jin, J. Y. Wang, W. Huang, *Appl. Phys. Lett.* **2016**, 108, 141102.
- [106] L. Gil-Escrig, G. Longo, A. Pertegas, C. Roldan-Carmona, A. Soriano, M. Sessolo, H. J. Bolink, *Chem. Commun.* **2015**, 51, 569.
- [107] L. Gil-Escrig, A. Miquel-Sempere, M. Sessolo, H. J. Bolink, *J. Phys. Chem. Lett.* **2015**, 6, 3743.
- [108] W. Nie, H. Tsai, R. Asadpour, J.-C. Blancon, A. J. Neukirch, G. Gupta, J. J. Crochet, M. Chhowalla, S. Tretiak, M. A. Alam, H.-L. Wang, A. D. Mohite, *Science* 2015, 347, 6221.
- [109] H.-L. Yip, Alex K.-Y. Jen, *Energy Environ. Sci.* **2012**, 5, 5994-6011
- [110] S. Chen, J. R. Manders, S.-W. Tsang, F. So, *J. Mater. Chem.*, **2012**, 22, 24202.
- [111] P. Schulz, E. Edri, S. Kirmayer, G. Hodes, D. Cahen, A. Kahn, *Energy Environ. Sci.* **2014**, 7, 1377.
- [112] Keith T. Butler, Jarvist M. Frost and Aron Walsh, *Mater. Horiz.*, 2015, 2, 228.
- [113] Y. Zhou, C. F. Hernandez, J. Shim, J. Meyer, A. J. Giordano, H. Li, P. Winget, T. Papadopoulos, H. Cheun, J. Kim, M. Fenoll, A. Dindar, W. Haske, E. Najafabadi, T. M. Khan, H. Sojoudi, S. Barlow, S. Graham, J.-L. Bredas, S. R. Marder, A. Kahn, B. A. Kippelen, *Science* **2012**, 336, 327.
- [114] G. Li, Z.-K. Tan, D. Di, M. L. Lai, L. Jian, J. H. W. Lim, R. H. Friend, N. C. Greenham, *Nano Lett.* **2015**, 15, 2640.
- [115] X. Qin, H. Doang, H. Hu, *Sci. China Mater.* 2015, 58, 186.
- [116] J. Li, S. G. R. Bade, X. Shan, Z. Yu, *Adv. Mater.* **2015**, 27, 5196.

- [117] J. C. Yu, D. B. Kim, E. D. Jung, B. R. Lee, M. H. Song, *Nanoscale*, **2016**, *8*, 7036.
- [118] S. G. R. Bade, J. Li, X. Shan, Y. Ling, Y. Tian, T. Dilbeck, T. Besara, T. Geske, H. Gao, B. Ma, K. Hanson, T. Siegrist, C. Xu, Z. Yu, *ACS Nano*, **2016**, *10*, 1795.
- [119] Z.-F. Shi, X.-G. Sun, D. Wu, T.-T. Xu, S.-W. Zhuang, Y.-T. Tian, X.-J. Li, G.-T. Du, *Nanoscale* 2016, **8**, 10035.
- [120] J. C. Yu, D. W. Kim, D. B. Kim, E. D. Jung, J. H. Park, A.-Y. Lee, B. R. Lee, D. D. Nuzzo, R. H. Friend, M. H. Song, *Adv. Mater.* **2016**, *28*, 6906.
- [121] Y.-H. Kim, H. Cho, J. H. Heo, S. H. Im, T.-W. Lee, *Current Applied Physics* **2016**, *16*, 1069.
- [122] G. L. Yang, H. Z. Zhong, *Chinese Chemical Letters* 2016, *27*, 1124.
- [123] Y. Ling, Z. Yuan, Y. Tian, X. Wang, J. C. Wang, Y. Xin, K. Hanson, B. Ma, H. Gao, *Adv. Mater.* **2016**, *28*, 305.
- [124] J. Xing, F. Yan, Y. Zhao, S. Chen, H. Yu, Q. Zhang, R. Zeng, H. V. Demir, X. Sun, A. Huan, Q. Xiong, *ACS Nano*, **2016**, *10*, 6623.
- [125] J. Song, J. Li, X. Li, L. Xu, Y. Dong, H. Zeng, *Adv. Mater.* **2015**, *27*, 7162-7167.
- [126] N. Yantara, S. Bhaumik, F. Yan, D. Sabba, H. A. Dewi, N. Mathews, P. P. Boix, H. V. Demir, Subodh Mhaisalkar, *J. Phys. Chem. Lett.* **2015**, *6*, 4360.
- [127] G. Li, F. W. R. Rivarola, N. J. L. K. Davis, S. Bai, T. C. Jellicoe, F. de la Peña, S. Hou, C. Ducati, F. Gao, R. H. Friend, N. C. Greenham, Z.-K. Tan, *Adv. Mater.* **2016**, *28*, 3528.
- [128] X. Zhang, B. Xu, J. Zhang, Y. Gao, Y. Zheng, K. Wang, X. W. Sun, *Adv. Funct. Mater.* **2016**, *26*, 4595.
- [129] H. Huang, H. Lin, S. V. Kershaw, A. S. Susa, W. C. H. Choy, A. L. Rogach, *J. Phys. Chem. Lett.* **2016**, *7*, 4398.
- [130] X. Zhang, C. Sun, Y. Zhang, H. Wu, C. Ji, Y. Chuai, P. Wang, S. Wen, C. Zhang, W. W. Yu, *J. Phys. Chem. Lett.* **2016**, *7*, 4602.

- [131] X. Zhang, H. Lin, H. Huang, C. Reckmeier, Y. Zhang, W. C. H. Choy, A. L. Rogach, *Nano Lett.* **2016**, *16*, 1415.
- [132] X. Zhanga, W. Wanga, B. Xua, S Liub, H. Daic, D. Biand, S. Chena, K. Wanga, X. W. Suna, *Nano Energy* **2017**, *37*, 40.
- [133] J. Li, L. Xu, T. Wang, J. Song, J. Chen, J. Xue, Y. Dong, B. Cai, Q. Shan, B. Han, H. Zeng, *Adv. Mater.* **2017**, *29*, 1603885.
- [134] J. Li, X. Shan, S. G. R. Bade, T. Geske, Q. Jiang, X. Yang, Zhibin Yu, *J. Phys. Chem. Lett.*, **2016**, *7*, 4059–4066
- [135] X. Zhang, B. Xu, W. Wang, S. Liu, Y. Zheng, S. Chen, K. Wang, X. W. Sun, *ACS Appl. Mater. Interfaces*, **2017**, *9*, 4926–493.
- [136] J. Pan, L. N. Quan, Y. Zhao, W. Peng, B. Murali, S. P. Sarmah, M. Yuan, L. Sinatra, N. M. Alyami, J. Liu, E. Yassitepe, Z. Yang, O. Voznyy, R. Comin, M. N. Hedhili, O. F. Mohammed, Z. H. Lu, D. H. Kim, E. H. Sargent, O. M. Bakr, *Adv. Mater.*, **2016**, *28*, 8718–8725
- [137] Y. Zhao, K. Zhu, *J. Phys. Chem. Lett.* **2014**, *5*, 4175.
- [138] N. J. Jeon, J. H. Noh, Y. C. Kim, W. S. Yang, S. Ryu, S. I. Seok, *Nat. Mater.* **2014**, *13*, 897.
- [139] M. Xiao, F. Huang, W. Huang, Y. Dkhissi, Y. Zhu, J. Etheridge, A. Gray-Weale, U. Bach, Y.-B. Cheng, L. A. Spiccia, *Angew. Chem.* **2014**, *126*, 10056.
- [140] J. H. Heo, D. H. Song, S. H. Im, *Adv. Mater.* **2014**, *26*, 8179.
- [141] S. Lee, J. H. Park, B. R. Lee, E. D. Jung, J. C. Yu, D. D. Nuzzo, R. H. Friend, M. H. Song, *J. Phys. Chem. Lett.* **2017**, *8*, 1784.
- [142] M. M. Lee, J. Teuscher, T. Miyasaka, T. N. Murakami, H. J. Snaith, *Science* **2012**, *338*, 643.
- [143] G. Sadoughi, D. E. Starr, E. Handick, S. D. Stranks, M. Gorgoi, R. G. Wilks, M. Baer, H. J. Snaith, *ACS Appl. Mater. Interfaces* **2015**, *7*, 13440.

- [144] M. Liu, M. B. Johnston, H. J. Snaith, *Nature* **2013**, *501*, 395.
- [145] C.-W. Chen, H.-W. Kang, S.-Y. Hsiao, P.-F. Yang, K.-M. Chian, H.-W. Lin, *Adv. Mater.* **2014**, *26*, 6647.
- [146] Q. Chen, H. Zhou, Z. Hong, S. Luo, H.-S. Duan, H.-H. Wang, Y. Liu, G. Li, Y. Yang, *J. Am. Chem. Soc.* **2014**, *136*, 622.
- [147] Y. Chen, T. Chen, L. Dai, *Adv. Mater.* **2015**, *27*, 1053.
- [148] N. K. Kumawat, N. Jain, A. Dey, K. L. Narasimhan, D. Kabra, *Adv. Funct. Mater.* **2016** (DOI: 10.1002/adfm.201603219)
- [149] Y-H Kim, H. Cho, T-W Lee, *Proc. Natl. Acad. Sci.* **2016**, *113*, 11694-11702
- [150] S. A. Veldhuis, P. P. Boix, N. Yantara, M. Li, T. C. Sum, N. Mathews, S. G. Mhaisalkar, *Adv. Mater.* **2016**, *28*, 6804–6834 .
- [151] T. Tachikawa, I. Karimata and Y. Kobori, *J. Phys. Chem. Lett.* **2015**, *6*, 3195-3201.
- [152] Y. Tian, A. Merdasa, M. Peter, M. Abdellah, K. Zheng, C. S. Ponseca Jr., T. Pullerits, A. Yartsev, V. Sundström, I. G. Scheblykin, *Nano Lett.*, **2015**, *15*, 1603–1608.
- [153] X. Li, F. Cao, D. Yu, J. Chen, Z. Sun, Y. Shen, Y. Zhu, L. Wang, Y. Wei, Y. Wu, H. Zeng, *Small*, **2017**, *13*, 1603996.
- [154] M. Kulbak, S. Gupta, N. Kedem, I. Levine, T. Bendikov, G. Hodes, D. Cahen, *J. Phys. Chem. Lett.*, **2016**, *7*, 167-172.
- [155] Y. Qu, M. Sliotsky, S. R. Forrest *Nature Photonics* **2015**, *9*, 758.
- [156] S. Moller, S. R. Forrest, *J. Appl. Phys.* **2002**, *91*, 3324.
- [157] M. H. Song, D. Kabra, B. Wenger, R. H. Friend, H. J. Snaith, *Adv. Funct. Mater.* **2009**, *19*, 2130.
- [158] M. Yuan, L. N. Quan, R. Comin, G. Walters, R. Sabatini, O. Voznyy, S. Hoogland, Y. Zhao, E. M. Beauregard, P. Kanjanaboos, Z. Lu, D. H. Kim, E. H. Sargent, *Nat. Nanotech.* **2016**, *11*, 872.

- [159] J. Byun, H. Cho, C. Wolf, M. Jang, A. Sadhanala, R. H. Friend, H. Yang, T.-W. Lee, *Adv. Mater.* **2016**, *28*, 7515.
- [160] Y. Kim, E. Yassitepe, O. Voznyy, R. Comin, G. Walters, X. Gong, P. Kanjanaboos, A. F. Nogueira, E. H. Sargent, *ACS Appl. Mater. Interfaces*, **2015**, *7*, 25007–25013.
- [161] G. Niu, X. Guo, L. Wang, *J. Mater. Chem. A*, **2015**, *3*, 8970.
- [162] Y. Rong, L. Liu, A. Mei, X. Li, H. Han, *Adv. Energy Mater.*, **2015**, *5*, 1501066
- [163] J-W. Lee, D-H Kim, H-S. Kim, S-W. Seo, S. M. Cho, N-G. Park, *Adv. Energy Mater.* **2015**, *5*, 1501310
- [164] B. Hailegnaw, S. Kirmayer, E. Edri, G. Hodes, D. Cahen, *J. Phys. Chem. Lett.*, **2015**, *6*, 1543–1547
- [165] L. Serrano-Lujan, N. Espinosa, T. T. Larsen-Olsen, J. Abad, A. Urbina, F. C. Krebs, *Adv. Energy Mater.*, **2015**, *5*, 1501119.
- [166] T. C. Jellicoe, J. M. Richter, H. F. J. Glass, M. Tabachnyk, R. Brady, S. E. Dutton, A. Rao, R. H. Friend, D. Credginton, N. C. Greenham, M. L. Böhm, *J. Am. Chem. Soc.*, **2016**, *138*, 2941–2944
- [167] N. K. Noel, S. D. Stranks, A. Abate, C. Wehrenfennig, S. Guarnera, A-A. Haghighirad, A. Sadhanala, G. E. Eperon, S. K. Pathak, M. B. Johnston, A. Petrozza, L. M. Herz, H. J. Snaith, *Energy Environ. Sci.*, **2014**, *7*, 3061-3068.
- [168] Y.-K. Chih, J.-C. Wang, R.-T. Yang, C.-C. Liu, Y.-C. Chang, Y.-S. Fu, W.-C. Lai, P. Chen, T.-C. Wen, Y.-C. Huang, C.-S. Tsao, T.-F. Guo, *Adv. Mater.* **2016**, *28*, 8687.
- [169] Zhao, B. Zhang, R. Zhao, B. Yao, X. Liu, J. Liu, Z. Xie, *J. Phys. Chem. Lett.* **2016**, *7*, 4259.
- [170] X. Ji, X. Peng, Y. Lei, Z. Liu, X. Yang, *Organic Electronics* **2017**, *43*, 167.
- [171] L. Zhao, J. Gao, Y. L. Lin, Y.-W. Yeh, K. M. Lee, N. Yao, Y.-L. Loo, B. P. Rand, *Adv. Mater.* **2017**, 1605317.

- [172] A. Sadhanala, A. Kumar, S. Pathak, A. Rao, U. Steiner, N. C. Greenham, H. J. Snaith, R. H. Friend, *Adv. Electron, Mater.* **2015**, 1, 1500008.
- [173] O. A. J.-Quintero, R. S. Sanchez, M. Rincon, I. Nora-Sero, *J. Phys. Chem. Lett.* **2015**, 6, 1883.
- [174] A. L. Palma, L. Cina, Y. Busby, A. Marsella, A. Agresti, S. Pescetelli, J.-J. Pireaux, A. D. Carlo, *ACS Appl. Mater. Interfaces*, **2016**, 8, 26989.